

See discussions, stats, and author profiles for this publication at: <https://www.researchgate.net/publication/323833019>

# Variability of East Asian summer monsoon precipitation during the Holocene and possible forcing mechanisms

Article in *Climate Dynamics* · January 2019

DOI: 10.1007/s00382-018-4175-6

CITATIONS

30

READS

1,540

11 authors, including:



Fuzhi Lu

Nanjing University

4 PUBLICATIONS 33 CITATIONS

[SEE PROFILE](#)



Chunmei Ma

Nanjing University

107 PUBLICATIONS 778 CITATIONS

[SEE PROFILE](#)



Cheng Zhu

60 PUBLICATIONS 838 CITATIONS

[SEE PROFILE](#)



Huayu Lu

Nanjing University

358 PUBLICATIONS 9,872 CITATIONS

[SEE PROFILE](#)

Some of the authors of this publication are also working on these related projects:




Estimation of Relative Pollen Productivity [View project](#)



40325007 National Natural Science Foundation of China [View project](#)

# Variability of East Asian summer monsoon precipitation during the Holocene and possible forcing mechanisms

Fuzhi Lu<sup>1</sup> · Chunmei Ma<sup>1,2</sup>  · Cheng Zhu<sup>1</sup> · Huayu Lu<sup>1,2</sup> · Xiaojian Zhang<sup>1</sup> · Kangyou Huang<sup>3</sup> · Tianhong Guo<sup>1</sup> · Kaifeng Li<sup>4</sup> · Lan Li<sup>5</sup> · Bing Li<sup>6</sup> · Wenqing Zhang<sup>7</sup>

Received: 29 September 2017 / Accepted: 13 March 2018  
© Springer-Verlag GmbH Germany, part of Springer Nature 2018

## Abstract

Projecting how the East Asian summer monsoon (EASM) rainfall will change with global warming is essential for human sustainability. Reconstructing Holocene climate can provide critical insight into its forcing and future variability. However, quantitative reconstructions of Holocene summer precipitation are lacking for tropical and subtropical China, which is the core region of the EASM influence. Here we present high-resolution annual and summer rainfall reconstructions covering the whole Holocene based on the pollen record at Xinjie site from the lower Yangtze region. Summer rainfall was less seasonal and ~30% higher than modern values at ~10–6 cal kyr BP and gradually declined thereafter, which broadly followed the Northern Hemisphere summer insolation. Over the last two millennia, however, the summer rainfall has deviated from the downward trend of summer insolation. We argue that greenhouse gas forcing might have offset summer insolation forcing and contributed to the late Holocene rainfall anomaly, which is supported by the TraCE-21 ka transient simulation. Besides, tropical sea-surface temperatures could modulate summer rainfall by affecting evaporation of seawater. The rainfall pattern concurs with stalagmite and other proxy records from southern China but differs from mid-Holocene rainfall maximum recorded in arid/semiarid northern China. Summer rainfall in northern China was strongly suppressed by high-northern-latitude ice volume forcing during the early Holocene in spite of high summer insolation. In addition, the El Niño/Southern Oscillation might be responsible for droughts of northern China and floods of southern China during the late Holocene. Furthermore, quantitative rainfall reconstructions indicate that the Paleoclimate Modeling Intercomparison Project (PMIP) simulations underestimate the magnitude of Holocene precipitation changes. Our results highlight the spatial and temporal variability of the Holocene EASM precipitation and potential forcing mechanisms, which are very helpful for calibration of paleoclimate models and prediction of future precipitation changes in East Asia in the scenario of global warming.

**Keywords** Holocene · EASM · Summer precipitation · CO<sub>2</sub> forcing · Ice volume forcing · Tropical forcing · ENSO · Pollen · Quantitative reconstruction · Climate modeling

---

**Electronic supplementary material** The online version of this article (<https://doi.org/10.1007/s00382-018-4175-6>) contains supplementary material, which is available to authorized users.

---

✉ Chunmei Ma  
chunmeima@nju.edu.cn

<sup>1</sup> School of Geographic and Oceanographic Sciences, Nanjing University, Nanjing 210023, Jiangsu, China

<sup>2</sup> Jiangsu Collaborative Innovation Center for Climate Change, Nanjing 210023, China

<sup>3</sup> School of Earth Sciences and Engineering, Sun Yat-Sen University, Guangzhou 510275, China

## 1 Introduction

The East Asian summer monsoon (EASM) is a subtropical monsoon that transports large amounts of heat and moisture to eastern China, Korea and Japan (Wang 2006). As a major

<sup>4</sup> College of Environment and Planning, Henan University, Kaifeng 475004, China

<sup>5</sup> School of History and Culture, Sichuan University, Chengdu 610064, China

<sup>6</sup> College of Resources and Environment, Hebei Normal University, Shijiazhuang 050024, China

<sup>7</sup> Center for Hydrogeology and Environmental Geology, China Geological Survey, Baoding 071051, China

component of the Earth's climate system, it now influences the lives of roughly one-fourth of the world's population (Lu et al. 2013a). Unlike the tropical Indian summer monsoon (ISM), the EASM exhibits complex rainfall structures that encompass tropics, subtropics, and mid-latitudes (Ding and Chan 2005; Wang et al. 2008). It has been found that the EASM rain belt has shifted southward in the last few decades, with more floods occurring in southern China, especially in the middle and lower reaches of Yangtze River, while more droughts happen in northern China (Ding et al. 2008; Sun et al. 2015). However, it remains unclear whether the observed southward migration of the EASM rain belt is induced by anthropogenic forcing or natural climate variability (Li et al. 2010; Yang et al. 2015a). The Holocene thermal maximum, a warm period at  $\sim 10\text{--}5$  cal kyr BP (Renssen et al. 2012), to some extent can be served as an analogue for global warming in the twenty-first century. Therefore, in order to predict future changes in the EASM rainfall under a warmer climate, it is crucial to understand the spatial and temporal variability of the EASM precipitation during the Holocene.

In recent decades, the variability of the EASM has been studied in detail by many researchers via various archives (An et al. 2015). Among these studies, speleothem  $\delta^{18}\text{O}$  records have been widely used as a proxy indicator of the EASM intensity on various timescales, with lower  $\delta^{18}\text{O}$  values implying higher spatially-integrated summer rainfall between the cave site and tropical Indo-Pacific oceans and/or higher local summer rainfall in the cave region (Cheng et al. 2012, 2016; Dykoski et al. 2005; Wang et al. 2001, 2005; Yuan et al. 2004). However, the correlation between rainfall and  $\delta^{18}\text{O}$  is extremely complex in the EASM region and therefore the climatic interpretation of speleothem  $\delta^{18}\text{O}$  records from Chinese cave deposits remains highly controversial (Tan 2014). Recent isotope-enabled modeling studies suggest that speleothem  $\delta^{18}\text{O}$  records do not represent summer rainfall in China during the Holocene and Heinrich events, but actually reflect isotopic composition of rainfall over the Indian Ocean and ISM region (LeGrande and Schmidt 2009; Pausata et al. 2011). To address this question, Liu et al. (2014b) proposed that the speleothem  $\delta^{18}\text{O}$  records are a robust proxy of the EASM intensity in terms of monsoonal airflow over eastern China and the accompanying summer precipitation in arid/semiarid northern China. However, this interpretation is challenged by independently-dated loess (Lu et al. 2013a), lake (Chen et al. 2015) and desert (Li et al. 2014b; Lu et al. 2005) records from arid/semiarid northern China, which all indicate a mid-Holocene rainfall/moisture maximum, being inconsistent with Chinese cave  $\delta^{18}\text{O}$  records (Liu et al. 2015). With that background in mind, one cannot infer past precipitation variability in East Asia directly from speleothem  $\delta^{18}\text{O}$  records unless independent quantitative records are available. Unfortunately,

quantitative rainfall reconstructions are extremely scarce for monsoonal China, especially for southern China.

The mei-yu (known as baiu in Japan and changma in Korea) is a nearly east–west-elongated summer rain band over the middle and lower reaches of Yangtze River, which is the most important rainfall-producing system of the EASM (Ding and Chan 2005; Wang et al. 2008). Wang et al. (2008) once assessed the meanings of twenty-five existing EASM indices and concluded that the mei-yu rainfall, which is produced in the primary rain-bearing system, the East Asian subtropical front, is the best indicator of the variability of EASM circulation system. However, the shortage of long-term rain gauge data has limited our ability to understand the mei-yu rainfall variability on longer timescales, e.g. during the Holocene. Although recently Li et al. (2017b) has presented a pollen-based quantitative reconstruction of annual precipitation covering the last 10 kyr for the lower Yangtze region, quantitative reconstructions of Holocene summer precipitation are still lacking for tropical and subtropical China, which is the core region of the EASM influence. Therefore, the Holocene evolution of mei-yu rainfall remains unresolved and needs further study.

In this study, we present a comprehensive dataset of quantitative rainfall records that contains seasonal signals, including total annual precipitation ( $P_{\text{ANN}}$ ), summer precipitation from May to September ( $P_{\text{MJJAS}}$ ) and summer precipitation from June to August ( $P_{\text{JJA}}$ ), based on pollen record at Xinjie site from the lower reaches of Yangtze River, which first extends instrumental records back to 12,500 years ago. Then we compare our reconstruction with a number of other rainfall-related Holocene records from both northern and southern China to investigate the spatial and temporal variability of the EASM rainfall (Fig. 1). We also investigate possible forcing mechanisms of Holocene EASM precipitation variability by comparing rainfall records with major drivers of Earth's climate system such as Northern Hemisphere summer insolation, high-northern-latitude ice volume, tropical sea-surface temperatures and greenhouse gas concentrations. It is interesting to find that our rainfall records coincide with paleoclimate records from humid southern China but differ from those in arid/semiarid northern China, indicating different rainfall responses between southern and northern China to high-northern-latitude ice volume forcing and tropical sea-surface temperature forcing during the Holocene. Hence, our study provides a valuable insight into the forcing and future variability of the EASM rainfall in a warming world.

## 2 Regional settings

The Xinjie site (119°42'E, 31°22'N; elevation 6 m above sea level) is located in the lower reaches of Yangtze River where mei-yu rainfall occurs (Fig. 1). Lying between warm

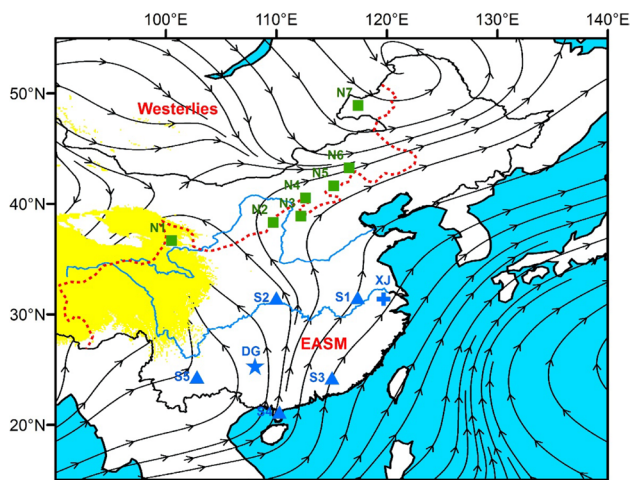


**Fig. 1** Rainfall patterns within the EASM domain during the Holocene synthesized by our study. June–July–August (JJA) mean 850-hPa streamlines based on NCEP reanalysis2 during 1979–2015 (Kanamitsu et al. 2002). Green squares (N1–N7) indicate locations of rainfall/moisture records in northern China with maximum rainfall/effective moisture occurred during the mid-Holocene at ~8–3 cal kyr BP. Blue triangles (S1–S5) indicate locations of rainfall/moisture records in southern China with maximum rainfall/effective moisture occurred during the early and middle Holocene at ~10–6 cal kyr BP (see Table 1 for details). The blue star indicates location of  $\delta^{18}\text{O}$  records from Dongge Cave (Dykoski et al. 2005; Wang et al. 2005). The blue cross indicates the location of Xinjie site in this study. Red dashed line indicates modern limit of Asian summer monsoon (400 mm isohyet). Areas where elevation is above 3000 m are shaded in yellow

temperate deciduous forest of northern China and subtropical evergreen forest of southern China (Supplementary Fig. S1) (Wu 1980), the natural vegetation is highly sensitive to precipitation/effective moisture changes induced by the EASM variability (An et al. 2000). Besides, there has continuous and thick lacustrine sediments widely distributed in the lowlands of this area (Zhu et al. 1987), which provides precious materials for the study of paleoclimate. The lower Yangtze region is also one of the most important cultural origins of Chinese civilization (Wu et al. 2012a; Zhu et al. 2014) where the earliest rice cultivation and domestication have been found (Zong et al. 2007; Zuo et al. 2017). Archaeological studies suggest that most Neolithic cultural sites are located in the southeastern part of the Taihu Plain (Zhu et al. 2003); whereas the western part has been less affected by human activities and natural landscapes were preserved until the last millennium (Okuda et al. 2003; Xu et al. 1995; Yi et al. 2006). Therefore, the pollen record from Xinjie site mainly reflects natural vegetation changes during most of the Holocene and is suitable for reconstructing past climate.

The modern climate at Xinjie site is characterized by two distinct seasons: (i) a cold and dry winter under the influence of the Siberian high-pressure system and the East Asian winter monsoon; (ii) a warm and wet summer

with the onset of the EASM and expansion of the western North Pacific subtropical high (An 2000). Mean annual temperature ( $T_{\text{ANN}}$ ) at the nearby Liyang meteorological station (31°26'N, 119°29'E; elevation 8 m above sea level) is 15.8 °C for the period 1953–2015, with mean coldest month temperature ( $T_{\text{COM}}$ ) of 2.8 °C and mean warmest month temperature ( $T_{\text{WAM}}$ ) of 28.4 °C. Mean annual precipitation ( $P_{\text{ANN}}$ ) is 1151 mm, most of which occur during summer time (Fig. 2). Mean precipitation of extended summer from May to September ( $P_{\text{MJJAS}}$ ) is 692 mm, accounting for ~60% of the  $P_{\text{ANN}}$ , while mean precipitation of meteorological summer from June to August ( $P_{\text{JJA}}$ ) is 480 mm, accounting for ~41% of the  $P_{\text{ANN}}$ .

### 3 Materials and methods

#### 3.1 Pollen analysis

The fieldwork was conducted in May 2013 and we obtained a 386 cm long core at Xinjie site (core LTD-12). Previously, a shorter pollen record (0–8 cal kyr BP) without climate reconstruction from core LTD-12 has been reported (Lu et al. 2015). For this study, we resampled this core at higher resolution and extended the pollen record to cover the whole of Holocene and the Younger Dryas (YD) period, and performed quantitative precipitation reconstructions. A total of 127 samples at 2 cm intervals from the top of core LTD-12 down to 379 cm were used for pollen analysis, with an average temporal resolution of 90 years per sample. Palynomorph extraction followed standard methods (Fægri and Iversen 1989). The procedures include HCl, KOH, HF and acetolysis treatments. A known number of *Lycopodium* spores were added prior to chemical treatment to calculate pollen concentrations. Identification followed pollen morphological atlases (Wang et al. 1995) aided by modern reference slides. A minimum of 500 terrestrial pollen grains were counted for each sample. Pollen percentages were calculated based on the total sum of terrestrial taxa. Pollen diagram was generated by the software Tilia version 2.04 (Grimm 1987). The fossil pollen data were summarized by a detrended correspondence analysis (DCA) (Hill and Gauch 1980) which copes well with non-linear species responses using CANOCO version 4.5 (Ter Braak and Smilauer 2002).

#### 3.2 Chronology

Ten composite  $^{14}\text{C}$  dates (Table 2) were used to construct an age-depth model for core LTD-12 (Supplementary Fig. S2). Four samples of core LTD-12 were directly dated by using the accelerator mass spectrometry (AMS)  $^{14}\text{C}$  technique, while the other six dates were cited from a parallel profile T5033 (Li et al. 2009). Rubidium contents of these two

profiles correlate well and hence the dating depths of T5033 were converted to the corresponding depths of core LTD-12 (Supplementary Fig. S3). The dating samples of core LTD-12 were prepared in the laboratory of Guangzhou Institute of Geochemistry, Chinese Academy of Sciences, and  $^{14}\text{C}$  was measured by the State Key Laboratory of Nuclear Physics and Technology, Peking University. The cited ages were dated using either conventional or AMS methods (CASS 1992; Li et al. 2009; Song et al. 1997). All  $^{14}\text{C}$  dates were calibrated to calendar years according to the software CALIB version 7.0.4 using the IntCal13 curve (Reimer et al. 2013). The ages of fossil pollen samples were calculated by linear interpolation or extrapolation. Although some of the dates were based on total organic carbon (TOC) which may suffer from old-carbon effects (Grimm et al. 2009), previous comparison with optically stimulated luminescence dating has confirmed their reliability (Li 2011).

### 3.3 Rainfall reconstructions

Our quantitative rainfall reconstructions are based on the weighted-averaging partial least squares (WAPLS) regression (Ter Braak and Juggins 1993), which combines the ability to model unimodal responses with efficient extraction of components (Birks 1998; Juggins and Birks 2012). WAPLS regression was selected because it has reliable predictive power and has been proven to perform as well as or even better than other numerical approaches in the practice of pollen-based reconstruction (Cao et al. 2014; Juggins and Birks 2012). Also, it has been widely applied to reconstruct past climate in many studies (Chen et al. 2014, 2015; Li et al. 2016, 2017a, b, c; Stebich et al. 2015; Xu et al. 2010). The model performance was evaluated by bootstrap cross-validation (Manly 2006). The optimal number of components was chosen by randomisation t test (van der Voet 1994) and represents a reduction in the root mean squared error of prediction by at least 5% (Birks 1998) (Supplementary Table S1). Sample-specific errors were estimated by bootstrap resampling with 1000 cycles (Birks 2003).

A total of 712 modern surface pollen samples located in the potential Holocene environment of Xinjie site were selected from the high-quality East Asian pollen database (Zheng et al. 2008, 2014) to form a modern training set (Supplementary Fig. S1). We excluded the surface pollen samples from deserts and steppes in northwestern China, as well as those from highland meadows on the Qinghai-Tibet Plateau according to the Holocene pollen assemblages at Xinjie site (Fig. 4 and Supplementary Fig. S4). We also excluded surface pollen samples from northeastern China because the persistent occurrence of *Tsuga* pollen suggests that the Holocene climate at Xinjie site cannot be as cold as current northeastern China (Supplementary Fig. S4) (Yang et al. 2009). Modern *Tsuga* is mainly found in the Southwest

Mountains (Hengduan Mountains), Southeast Mountains, Central Mountains (Qinling and Daba Mountains), Taiwan Central Range, and Japanese Archipelago (except Hokkaido); in contrast, no *Tsuga* is found in northeastern China (Yang et al. 2009). Therefore, surface pollen samples from northeastern China should not be considered as an analogue. The continental-scale East Asian pollen database has been shown to be powerful and suitable for WAPLS models (Cao et al. 2014; Li et al. 2015; Lu et al. 2011a; Zheng et al. 2014). It has been checked that every fossil pollen sample has its closest analogue in the modern training set. Pollen percentages were calculated based on total terrestrial taxa sum and square-root transformed to improve the ratio of signal to noise (Prentice 1980). The three target climate variables to be reconstructed are  $P_{\text{ANN}}$ ,  $P_{\text{MJJAS}}$  and  $P_{\text{JJA}}$ , because they are ecologically meaningful (Cao et al. 2014) and correlated directly with the EASM (Wang et al. 2012). For the EASM region, the total annual precipitation is dominated by the summer precipitation (Ding and Chan 2005). However, summer precipitation might have a stronger influence on Holocene vegetation than annual precipitation, because summer precipitation occurs in a warm season when plants grow and thereby is more biologically meaningful. Modern rainfall values were extracted from the WorldClim version 2 database at a very high spatial resolution ( $\sim 0.86 \text{ km}^2$ ) for the period 1970–2000 (Fick and Hijmans 2017). The accuracy of the WorldClim version 2 database has been improved by using satellite data (Fick and Hijmans 2017). The rainfall data were  $\log_{10}(X + 1)$  transformed before modeling since they exhibit log-normal distributions (Juggins and Telford 2012).

A novel method (Telford and Birks 2011) was used to assess the statistical significance of the quantitative rainfall reconstructions, which shows that all three rainfall variables are statistically significant (Fig. 3). The reconstruction of annual precipitation can explain 31% of the variance in the fossil pollen data and is better than 98% of the reconstructions trained on random environmental variables. For the two summer precipitation reconstructions,  $P_{\text{MJJAS}}$  and  $P_{\text{JJA}}$  can explain 32 and 33% of the variance in the fossil pollen data at Xinjie site, respectively; which is better than 99% of the reconstructions trained on random environmental variables, supporting our assumption that summer precipitation might have a stronger influence on Holocene vegetation in the lower Yangtze region than total annual precipitation. Since temperature and precipitation are the most significant variables that control regional vegetation, we also assessed the statistical significance of temperature reconstructions. The results show that reconstructions of temperature variables ( $T_{\text{ANN}}$ ,  $T_{\text{COM}}$ ,  $T_{\text{WAM}}$ ) at Xinjie site can explain less variances in the fossil data than those of precipitation reconstructions, further supporting that our precipitation reconstructions are reliable (Fig. 3).

### 3.4 Climate model simulations

In order to investigate the possible forcing mechanisms behind the EASM precipitation variability, we compared our precipitation reconstructions with model results from the Paleoclimate Modeling Intercomparison Project (PMIP) (Fig. 9) (Joussaume and Taylor 1995). For the mid-Holocene experiment of the PMIP, the core forcing lies in orbitally-induced ~5% changes in the seasonal distribution of solar insolation (Berger 1978). More details on the models and data were given by Jiang et al. (2013). In order to investigate the individual and combined effects of various climate forcings on the EASM precipitation, we also compared our precipitation reconstructions with model results from the TraCE-21 ka transient simulation, which simulated continuous climate evolution of the last 21 kyr (Liu et al. 2009, 2014b). The TraCE-21 ka simulation was performed in a state-of-art coupled ocean-atmosphere model, the Community Climate System Model version 3 (CCSM3) of the National Center for Atmospheric Research with a spatial resolution of T31 (3.75° × 3.75°) (Collins et al. 2006). The full TraCE simulation was driven by the complete set of realistic transient climate forcing, including orbitally-induced solar insolation variations (Berger 1978), atmospheric greenhouse gas concentrations (Joos and Spahni 2008), meltwater fluxes (Liu et al. 2009) and continental ice sheets (Peltier 2004). The full TraCE simulation can capture many key characteristics of the reconstructed climate evolution such as the Bølling-Allerød warming (Liu et al. 2009), the Younger Dryas cooling (Liu et al. 2012) and El Niño variability (Liu et al. 2014a). Four single-forcing transient simulations (ORB, GHG, ICE and MWF) were conducted in the same way as the full TraCE simulation, but each was driven by a single forcing with other transient forcings and boundary conditions remaining constant at the start of each simulation (He et al. 2013). Simulations ORB and GHG were initialized from the full TraCE state at 22 cal kyr BP. ORB was driven only by transient variations in orbital configuration (Berger 1978); while GHG was driven only by transient variations in greenhouse gas concentrations (Joos and Spahni 2008). Simulations ICE and MWF were initialized at the full TraCE state of 19 cal kyr BP. ICE was driven only by the changing continental ice sheets (Peltier 2004); while MWF was driven only by transient variations in the Northern Hemisphere meltwater fluxes (Liu et al. 2009). We calculated the regional-averaged summer precipitation in the region (28–38°N; 112–124°E) around Xinjie site for southern China and calculated the regional-averaged summer precipitation in the region (38–53°N; 80–105°E) over deserts and drylands for arid/semiarid northern China (Supplementary Fig. S5). These regions are in well agreement with the spatial distribution of proxy records synthesized (Fig. 1) and the modeled summer precipitation changes can be representative

of the reconstructed precipitation changes from geological records (Fig. 7). However, the regions are not exactly identical to the traditional view of southern China and northern China divided by the Qinling-Huaihe line (~34°N). This is because the spatial resolution of TraCE-21 ka simulation is too low to divide southern and northern China in an accuracy way. Besides, the thermal equator of TraCE-21 ka simulation has been found to be situated more North than the true by ~4° (Shanahan et al. 2015) and thereby it cannot correctly capture the spatial patterns of reconstructed precipitation changes if the traditional division of southern China and northern China was used directly without any adjustments (Liu et al. 2014b). It is known that precipitation field is much difficult to simulate and subject to great model errors (Liu et al. 2014b). In order to evaluate the relative importance of summer insolation forcing and greenhouse gas forcing in influencing Holocene summer precipitation at Xinjie site in southern China, we compared simulations ORB and GHG in a more detail way by calculating their absolute contributions (Fig. 12). The absolute contributions were calculated by subtracting summer precipitation in the full TraCE state at 22 cal kyr BP. This is the time when ORB and GHG were initialized with other transient forcings and boundary conditions remaining constant. Therefore, summer rainfall at that time is the baseline for calculating their absolute contributions.

## 4 Results and discussion

### 4.1 Vegetation succession in the lower yangtze region

The pollen diagrams (Fig. 4 and Supplementary Fig. S4) show clear changes in natural vegetation of the lower Yangtze region since ~12.5 cal kyr BP. From ~12.5 to 11.5 cal kyr BP, *Artemisia* increased rapidly while *Cyclobalanopsis* and *Quercus* decreased significantly. Maximum values of conifer and steppe taxa (*Pinus* and *Artemisia*) and minimum values of broadleaved arboreal taxa (*Cyclobalanopsis*, *Liquidambar* and *Quercus*) indicate a cold and dry climate prevailing in the period of the Younger Dryas (Carlson 2013). After ~11.5 cal kyr BP, the percentages of subtropical arboreal taxa (*Cyclobalanopsis* and *Liquidambar*) and deciduous *Quercus* increased abruptly, indicating rapid warming of the climate and strengthening of the EASM at the start of Holocene (Dong et al. 2010; Johnsen et al. 2001). From ~11.5 to 4.2 cal kyr BP, the pollen assemblages were dominated by *Cyclobalanopsis*, *Liquidambar* and *Quercus*, implying a mixed forest consisting of evergreen and deciduous broadleaved trees under a warmer and wetter climate during the early and middle Holocene. After ~5.5 cal kyr BP, *Pinus* increased gradually at the expense of evergreen

broadleaved trees, which may be in response to the gradual cooling of climate and weakening of the EASM (Marcott et al. 2013; Wang et al. 2005). During the mid- to late Holocene transition, the vegetation experienced an abrupt shift at  $\sim 4.2$  cal kyr BP with the replacement of subtropical evergreen and deciduous broadleaved forest by a cold-tolerant forest community dominated by *Pinus*. The general trend of vegetation succession at Xinjie site is further supported by the scores of DCA axis 1 (Fig. 4). The Holocene vegetation history at Xinjie site is in good agreement with many other published pollen records from the lower Yangtze region (Chen et al. 2009; Innes et al. 2014; Liu et al. 1992; Okuda et al. 2003; Shu et al. 2007; Xu et al. 1995; Yang et al. 1996; Yao et al. 2017a; Yi et al. 2006). It is also consistent with a large number of pollen records from tropical and subtropical China (Dearing et al. 2008; Kramer et al. 2010; Sheng et al. 2017; Wang et al. 2007; Xiao et al. 2007; Zhao et al. 2009, 2017; Zhu et al. 2010). These coherent variations among pollen records covering a broad geographical region are better explained by climate change than by human impact (Innes et al. 2014; Zhao et al. 2009). However, human disturbance may have been intense enough to destroy natural vegetation over the last millennium, as indicated by reduction in tree pollen such as *Pinus* and sharp increase in herbaceous pollen such as Poaceae and Brassicaceae (Cao et al. 2010; Li et al. 2014a; Lu et al. 2015). Some previous studies also suggest that human influence was insignificant in the west Taihu basin before the last millennium (Okuda et al. 2003; Yao et al. 2017a).

## 4.2 Precipitation variability in the lower yangtze region

The pollen-based quantitative reconstructions of three rainfall variables ( $P_{ANN}$ ,  $P_{MJAS}$  and  $P_{JJA}$ ) with sample-specific errors as well as rainfall seasonality are shown in Fig. 5. Therefore, here we provide a high-resolution dataset of Holocene precipitation changes for the lower reaches of Yangtze River, which reveals not only annual rainfall variability but also summer rainfall variability. Reconstructed precipitation shows low values during the YD period and increases abruptly at the start of the Holocene, maintaining high values until  $\sim 6$  cal kyr BP (about 20–30% higher precipitation than present), followed by a gradual decrease. Since  $\sim 4.2$  cal kyr BP, the precipitation does not decrease monotonically but exhibits strong oscillations of multi-centennial duration. In general, the annual precipitation and summer precipitation have varied synchronously on various time scales ranging from several decades to ten thousands of years. Our calculation of rainfall seasonality shows that the mean contributions of the  $P_{MJAS}$  and  $P_{JJA}$  to the  $P_{ANN}$  during the Holocene are  $\sim 71\%$  and  $\sim 48\%$ , respectively (Fig. 5d, e), indicating that the annual precipitation at Xinjie site has

been dominated by the EASM precipitation throughout the Holocene. However, the rainfall seasonality also changed with time over the past 12.5 kyr. During the early and middle Holocene, the contribution of summer precipitation to the annual precipitation was relatively small, compared to the late Holocene and Younger Dryas period, indicating that the precipitation was less seasonal in the early and middle Holocene when the climate was warm and wet but became more seasonal in the late Holocene and Younger Dryas when the climate was cool and dry. This might be because that, during the early and middle Holocene, the rainy season became longer while the dry season became shorter, similar to the current tropical rainforest climate (Peel et al. 2007), which could be best explained by the northward migration of the Intertropical Convergence Zone (Haug et al. 2001). On the centennial to millennial timescales, the general trend of rainfall was punctuated by several dry events such as 4.2-kyr event, 7.0-kyr event and 9.0-kyr event. These events coincide with weak Asian monsoon events inferred from speleothem  $\delta^{18}O$  records at Dongge Cave (Dykoski et al. 2005; Wang et al. 2005) and can be correlated to ice-rafting events in the North Atlantic (Bond et al. 1997, 2001). The 4.2-kyr event has been documented by many proxy records in eastern China (Innes et al. 2014; Ma et al. 2008; Yang et al. 2015b; Yao et al. 2017a) and may have been responsible for the collapse of Neolithic cultures such as the Liangzhu Culture (Wu and Liu 2004). The 9.0-kyr event is considered to be a widespread climate anomaly across the whole Northern Hemisphere with cooling at high latitudes and drying in the tropics (Fleitmann et al. 2008). Therefore, it seems that the Holocene precipitation in the lower Yangtze region was susceptible to global climate change. Besides, the dry events correspond to intervals of strong seasonality, indicating that rainy season was much shorter and summer precipitation was more concentrated during dry periods, which may imply that both drought and flood could happen in the same year.

## 4.3 Broad-scale controls on summer precipitation at xinjie site

To investigate the factors that directly and indirectly control the precipitation changes at Xinjie site during the Holocene, we compare our reconstruction with proxy records of broad-scale atmospheric circulations such as the EASM and the Intertropical Convergence Zone (ITCZ) (Fig. 6). Note that the speleothem  $\delta^{18}O$  record is generally considered to represent broad-scale atmospheric circulation rather than EASM precipitation, because its relationship with rainfall is complex and debated (Liu et al. 2014b; Maher and Thompson 2012; Tan 2014; Zhang et al. 2017). Overall, the temporal pattern of summer rainfall at Xinjie site bears a remarkable resemblance to high-resolution  $\delta^{18}O$  records from Dongge Cave (Dykoski et al. 2005; Wang et al. 2005), to

titanium concentration data from the Cariaco Basin (Haug et al. 2001), and to temperature anomalies in the extratropical Northern Hemisphere (30°–90°N) (Marcott et al. 2013). These strong similarities demonstrate that summer precipitation at Xinjie site is tightly linked to the EASM circulation system and to the mean position of the ITCZ during the Holocene at orbital timescales, with high rainfall corresponding to strong monsoonal circulation and northward movement of the ITCZ. Besides, temperature changes in the Northern Hemisphere may have been an important driving force of the EASM circulation system and ITCZ migration (Lu et al. 2013a; Schneider et al. 2014). Variations in the thermal gradient between Northern and Southern Hemisphere lead to meridional movements of the ITCZ and EASM rain belt (Lu et al. 2013a; Schneider et al. 2014), and thus influence summer precipitation at Xinjie site. However, temperature change and ITCZ migration cannot explain all variability of the EASM circulation system and summer rainfall at Xinjie site, because their late-Holocene evolutions are quite different. For example, the temperature continued to decline and the ITCZ continued to shift southward during the late Holocene. In contrast, monsoonal circulation indicated by Dongge cave  $\delta^{18}\text{O}$  records (Dykoski et al. 2005; Wang et al. 2005) and summer precipitation at Xinjie site remained constant and/or even increased over the last few millennia. Therefore, another broad-scale atmospheric circulation, in addition to the ITCZ, must have played a key role in modulating the EASM circulation system and associated summer rainfall. Because the western North Pacific (WNP) subtropical high is a major and important component of the present-day EASM circulation system (Ding and Chan 2005; Wang et al. 2008), we argue that the WNP subtropical high might have influenced the EASM circulation system and summer rainfall at Xinjie site during the late Holocene too. Although there is a strong coherency between the speleothem  $\delta^{18}\text{O}$  records and summer precipitation at Xinjie site during the Holocene, a major deviation is noted over the last millennium. The speleothem  $\delta^{18}\text{O}$  records increase remarkably, known as “the 2-kyr shift” (Cheng et al. 2016), but the upward trend of summer precipitation at Xinjie site is less marked. This may be attributable to intense human impact as reflected by the pollen record.

#### 4.4 Different rainfall patterns between southern and northern China

Higher summer rainfall during the early and middle Holocene than the late Holocene at Xinjie site is consistent with independent paleoclimate records from monsoonal South China (shown in Fig. 1 and listed in Table 1). For instance, high-resolution evidence from eutrophic peat/mud sequences at Dahu, Jiangxi Province, indicates that the Holocene optimum of the EASM precipitation occurred between ~10 and

6 cal kyr BP in southern China (Zhou et al. 2004). Additionally, a semi-quantitative synthesis of many pollen records with reliable chronologies and high-resolution data from southern China suggests a humid climate in the early and middle Holocene, but a drier climate in the late Holocene (Fig. 6e) (Zhao et al. 2009). More recently, Li et al. (2017b) present a quantitative annual rainfall reconstruction based on pollen from Chaohu Lake (Fig. 6d, green), ~220 km west of Xinjie site, which shows a similar trend to the inferred rainfall at Xinjie site. However, two hydrological records from Dajiuhu peatland and Heshang Cave in the middle Yangtze region indicate wet conditions in the early and late Holocene, but dry conditions in the mid-Holocene (Xie et al. 2013). These two records are also inconsistent with other proxy records from the same sites, including a pollen record from Dajiuhu peatland (Zhu et al. 2010) and a speleothem  $\delta^{18}\text{O}$  record from Heshang Cave (Hu et al. 2008). This discrepancy may occur for a number of reasons such as climatic sensitivity of the different proxy indicators (Li et al. 2017b). A recent study from the same site (Heshang Cave) has related the two hydrological records to extreme events such as storms and floods (Zhu et al. 2017). In summary, the quantitative reconstruction of precipitation at Xinjie site together with the evidence outlined above indicate that southern China has experienced a declining monsoonal rainfall pattern during the Holocene.

However, this rainfall pattern does not agree with rainfall records from the currently arid and semiarid northern China (Chen et al. 2015; Li et al. 2014b; Lu et al. 2005, 2013a), which indicate a mid-Holocene maximum rainfall at ~8–3 cal kyr BP (Fig. 6f, g). For example, a well-dated, high-resolution annual rainfall reconstruction based on pollen record from Gonghai Lake in northern China indicates that the rainfall maximum occurred during the mid-Holocene (Fig. 6f, blue) (Chen et al. 2015). A reconstruction of summer precipitation since ~9.5 cal kyr BP for northern China exhibits a similar trend, with inferred maximum rainfall at ~7–4 cal kyr BP (Fig. 6f, green) (Li et al. 2016). In addition, proxy records of loess magnetic susceptibility, total organic carbon and organic carbon isotopic composition from the Chinese Loess Plateau, which are considered to be directly linked to summer rainfall, suggest a more humid climate at ~8–3 cal kyr BP (Lu et al. 2013a). Moreover, a reconstruction of effective moisture levels based on sedimentary facies and vegetation types from deserts and sandy lands of northern China indicates that the climate gradually became wetter between ~12 and 6 cal kyr BP, reaching a maximum effective moisture at ~8–3 cal kyr BP (Fig. 6g) (Li et al. 2014b; Lu et al. 2013b). Therefore, the summer rainfall in northern China has a unimodal pattern during the Holocene, which is distinct from that in southern China (Fig. 7). Another major difference lies in the late Holocene. After ~3.3 cal kyr BP, the summer precipitation in arid/



**Table 1** List of sites of rainfall/moisture records shown in Fig. 1 and discussed in the text

Site ID	Site name	Latitude (°N)	Longitude (°E)	Region	Proxy type	Dating method	Number of dates	References
N1	Qinghai Lake	36.67	100.51	North China	Pollen-based precipitation	AMS	7	Li et al. (2017a) and Shen et al. (2005)
N2	Yulin section	38.33	109.73	North China	Loess magnetic susceptibility	OSL	4	Lu et al. (2013a)
N3	Gonghai Lake	38.9	112.23	North China	Pollen-based precipitation	AMS	22	Chen et al. (2015)
N4	Daihai Lake	40.55	112.66	North China	Pollen-based precipitation	AMS	8	Li et al. (2016); Xiao et al. (2004) and Xu et al. (2010)
N5	Bayanchagan Lake	41.65	115.21	North China	Tree pollen percentage	AMS	6	Jiang et al. (2006)
N6	Dali Lake	43.26	116.6	North China	Pollen-based precipitation	AMS	18	Xiao et al. (2015)
N7	Hulun Lake	48.92	117.42	North China	Pollen-based precipitation	AMS	13	Wen et al. (2010)
S1	Chaohu Lake	31.53	117.37	South China	Pollen-based precipitation	AMS	10	Chen et al. (2009) and Li et al. (2017b)
S2	Dajiuhu Peat	31.49	110	South China	Evergreen tree pollen percentage, carbon isotope	AMS	7	Ma et al. (2008); Ma et al. (2009) and Zhu et al. (2010)
S3	Dahu Peat	24.25	115.03	South China	Evergreen tree pollen percentage	AMS	12	Xiao et al. (2007) and Zhou et al. (2004)
S4	Huguangyan Lake	21.15	110.28	South China	Tropical tree pollen percentage, chlorophyll a	AMS	12, 7, 24	Sheng et al. (2017); Wang et al. (2007) and Wu et al. (2012b)
S5	Xingyun Lake	24.34	102.8	South China	Pollen-based precipitation	AMS	8	Chen et al. (2014)
DG	Dongge Cave	25.28	108.08	South China	Speleothem $\delta^{18}\text{O}$	$^{230}\text{Th}$	37, 45	Dykoski et al. (2005) and Wang et al. (2005)

semiarid northern China decreased rapidly (Chen et al. 2015), faster than the decrease in the Northern Hemisphere summer insolation (Laskar et al. 2004). In contrast, the summer precipitation in southern China remained unchanged and/or even increased in an anomalous fashion over the last two millennia, deviated from the downward trend of summer insolation in the Northern Hemisphere (Laskar et al. 2004). Our finding of different rainfall patterns between southern China and currently arid/semiarid northern China is supported by the full TraCE simulation (Liu et al. 2009), which shows that modeled summer precipitation in the region around Xinjie site was highest in the period from 10 to 6 cal kyr BP while the modeled summer precipitation in

arid/semiarid northern China was highest during the mid-Holocene (Fig. 7a, c).

#### 4.5 Possible forcing mechanisms for EASM rainfall variability

To test for links between EASM precipitation and major climate forcings, we compare summer rainfall records from southern and northern China to July insolation at 65°N (Laskar et al. 2004), arctic ice-sheet extent (Dyke 2004), fresh-water flux in the Northern Hemisphere (Liu et al. 2014b), an Atlantic meridional overturning circulation (AMOC) proxy in the subtropical North Atlantic

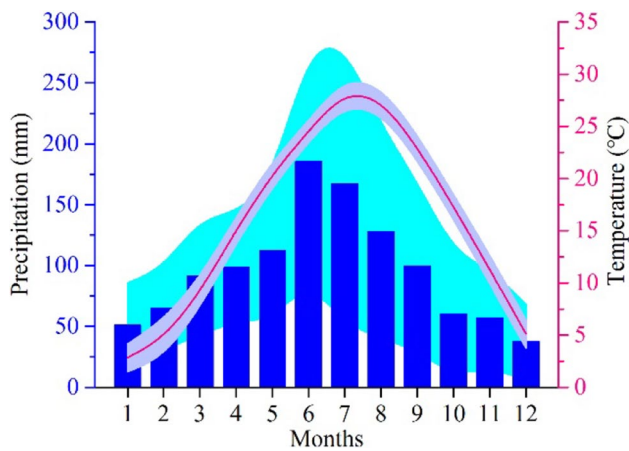


**Fig. 2** Monthly mean temperature and monthly total precipitation from the Liyang meteorological station calculated over the period 1953–2015. The shaded areas denote standard deviations

Ocean (McManus et al. 2004), sea-level rise in the western Pacific (Liu et al. 2004), sea-surface temperatures of the Indo-Pacific Warm Pool (Stott et al. 2004), El Niño/Southern Oscillation (ENSO) variability in the equatorial eastern Pacific (Moy et al. 2002), and atmospheric carbon dioxide (CO<sub>2</sub>) and methane (CH<sub>4</sub>) concentrations from Antarctica (Loulergue et al. 2008; Luthi et al. 2008) (Fig. 8). These various climate forcings can be divided into four main groups: (i) summer insolation forcing; (ii) high latitude forcing (ice sheet, sea-level change, fresh water flux, AMOC); (iii) low latitude forcing (tropical sea-surface temperatures, ENSO variability); and (iv) greenhouse gas forcing (CO<sub>2</sub> and CH<sub>4</sub> concentrations).

#### 4.5.1 Insolation forcing

Changes in the Earth's orbital parameters (i.e., eccentricity, obliquity and precession) modulate the seasonal distribution

of solar insolation. A number of loess and speleothem records reveal that the long-term history of the EASM is dominated by orbital cycles (Cheng et al. 2012; Lu et al. 2004), indicating that the EASM is subject to insolation forcing at orbital time scales. The summer rainfall at Xinjie site varies broadly in concert with changes in July insolation at 65°N (Laskar et al. 2004), supporting the hypothesis of insolation forcing (Fig. 8d) (Kutzbach 1981; Kutzbach and Guetter 1986). Higher summer insolation during the early and middle Holocene induced stronger ocean-to-land thermal gradients, which enhanced monsoon circulation and brought more water vapour to the lower reaches of the Yangtze River, in favor of more summer precipitation. In contrast, the decrease of summer rainfall during the mid- to late Holocene was in response to the lowering of Northern Hemisphere summer insolation (Laskar et al. 2004). Most model results from the Paleoclimate Modeling Intercomparison Project (PMIP) suggest that mid-Holocene summer precipitation was ~10% higher than the baseline period in the EASM region due to orbital forcing (Jiang et al. 2013). However, the PMIP model results underestimate the magnitude of reconstructed summer rainfall variation (Fig. 9). In addition, the PMIP models simulate decreased mid-Holocene annual rainfall in the middle and lower reaches of the Yangtze and Yellow Rivers (Jiang et al. 2013), which is in conflict with geological records. Therefore, our precipitation reconstructions potentially provide evidence for the validation and correction of climate models. Furthermore, insolation forcing on the EASM precipitation is supported by the TraCE transient simulation, which shows that the regional-averaged summer precipitation in the region around Xinjie site decreased from the early Holocene to the late Holocene mainly due to summer insolation forcing (Fig. 10).

Insolation change, however, is unlikely to be the only control on the EASM precipitation, because reconstructed summer rainfall at Xinjie site was punctuated by several dry events such as the Younger Dryas event during a time when

**Table 2** Radiocarbon dates used for the chronology of core LTD-12 at Xinjie site

Laboratory code	Dated material	Dating method	Depth (cm)	<sup>14</sup> C date (years BP)	Calibrated age (cal years BP) (2σ)	References
GZ6724	TOC	AMS	50.5	2120 ± 25	2002–2152	This study
BK95045	Charcoal	<sup>14</sup> C	110.0	3340 ± 65	3442–3722	Song et al. (1997)
ZK0254	Charcoal	<sup>14</sup> C	150.0	3840 ± 95	3978–4448	CASS (1992)
SH0030	Charcoal	<sup>14</sup> C	182.0	4320 ± 70	4805–5067	CASS (1992)
KF071204	TOC	<sup>14</sup> C	231.0	5281 ± 175	5696–6398	Li (2011)
XA3318	Peat	AMS	240.0	5903 ± 26	6666–6759	Li (2011)
XA3323	Peat	AMS	269.0	6266 ± 28	7161–7260	Li (2011)
GZ6730	TOC	AMS	299.5	7310 ± 30	8032–8179	This study
GZ6731	TOC	AMS	339.5	9060 ± 45	10,169–10,285	This study
GZ6732	TOC	AMS	385.5	11,135 ± 45	12,853–13,097	This study

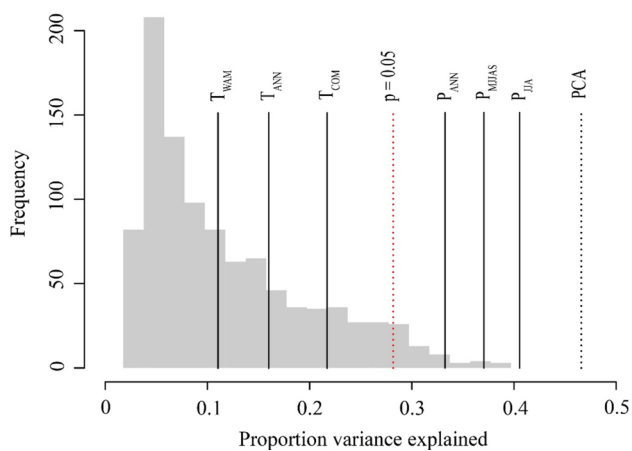


**Fig. 3** Histogram of the proportion of variance in the LTD-12 pollen record explained by 999 transfer functions (WAPLS-2) trained with random environmental data. Solid black lines mark the proportions of variance explained by  $T_{ANN}$ ,  $T_{COM}$ ,  $T_{WAM}$ ,  $P_{ANN}$ ,  $P_{MJJAS}$  and  $P_{JJA}$ . Black dotted line marks the proportion of variance explained by the first axis of a principal components analysis (PCA) of the fossil pollen data. Red dotted line marks the proportion of variance below which 95% of the reconstructions trained on random environmental variables can explained ( $p=0.05$ )

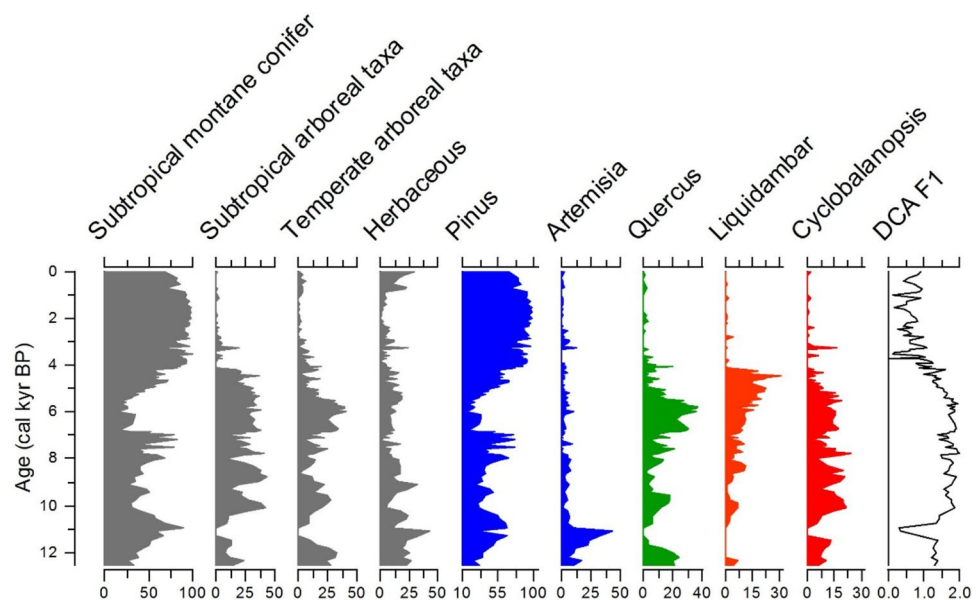
summer insolation was high. Besides, as observed in the precipitation/effective moisture records from northern China (Chen et al. 2015; Li et al. 2014b; Liu et al. 2015; Lu et al. 2005, 2011b, 2013a; Xu et al. 2010), the maximum rainfall/effective moisture significantly lags peak insolation by ~4–5 kyr. Furthermore, the inferred summer precipitation at Xinjie site deviates from the downward trend of summer insolation during the late Holocene. To explain these discrepancies, we hypothesize that during the last deglaciation

and early Holocene when glacial boundary conditions were still strong, high-northern-latitude ice volume in addition to summer insolation change might have influenced the spatial and temporal variability of the EASM precipitation. During the late Holocene when summer insolation forcing was weak, tropical sea-surface temperatures (especially ENSO) and greenhouse gas concentrations might have offset or promoted the effect of insolation forcing.

#### 4.5.2 High latitude forcing

Variations in high-northern-latitude ice volume have been considered to influence the EASM and East Asian winter monsoon (EAWM) on glacial-interglacial time scales (Ding et al. 1995, 2002; Ding and Yu 1995; Liu and Ding 1992), but how it influences the spatial and temporal variability of EASM precipitation during the Holocene is poorly understood. The development of ice volume in high northern latitudes causes lowering of the global sea level, increase in the land-surface albedo, enhancement of the Siberian high, strengthening of the EAWM and southward displacement of the Westerlies (Chen and Huang 1998; Ding et al. 1995, 2002; Ding and Yu 1995; Hao et al. 2012; Liu and Ding 1992). During the last deglaciation and early Holocene, the ice volume in the Northern Hemisphere was still large and global sea level was low (Fig. 8a, b) (Dyke 2004; Liu et al. 2004). The high-northern-latitude ice volume might affect the EASM precipitation by means of three key processes (Ding et al. 2005). First, the lowering of sea level and subsequent exposure of East Asian continental shelves in the Pacific marginal seas increases the distance for moisture transport from ocean to land, thereby reducing the summer rainfall over northern China and allowing deserts and

**Fig. 4** Pollen percentage diagram of key pollen types at Xinjie site and detrended correspondence analysis (DCA) axis 1 scores. See Fig. S4 in the supplementary material for more details



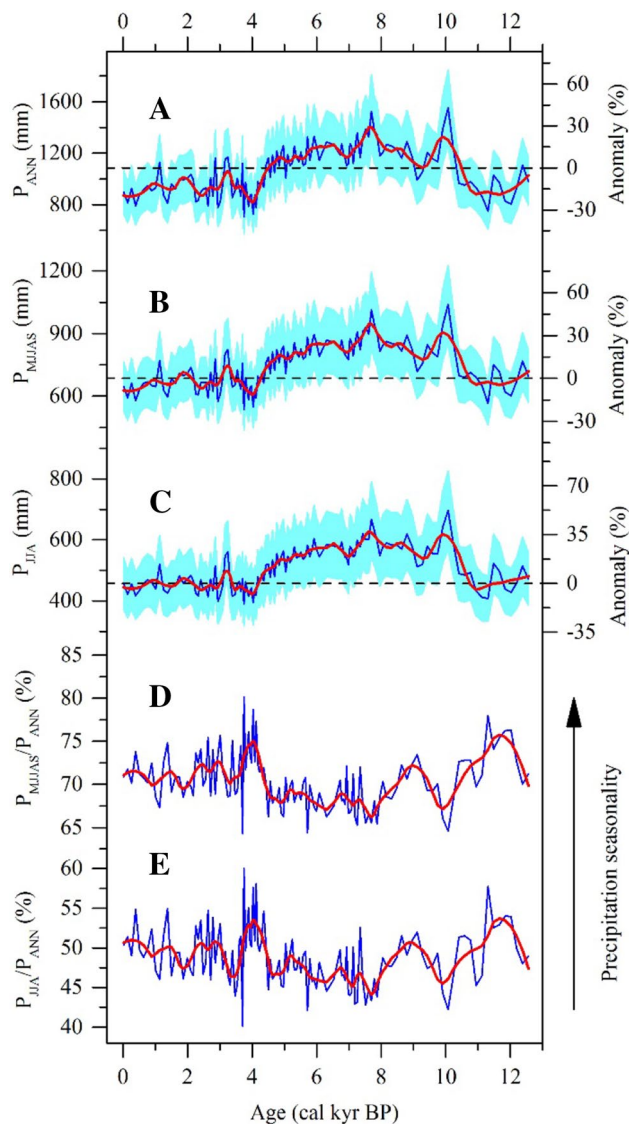


**Fig. 5** Pollen-based quantitative reconstructions of precipitation change and seasonality at Xinjie site. **a** Annual precipitation ( $P_{ANN}$ ). **b** Extended summer precipitation from May to September ( $P_{MJJAS}$ ). **c** Summer precipitation from June to August ( $P_{JJA}$ ). **d** Contribution of  $P_{MJJAS}$  to  $P_{ANN}$ . **e** Contribution of  $P_{JJA}$  to  $P_{ANN}$ . Cyan bands in plots **a–c** indicate bootstrap-estimated standard errors. Red lines in plots **a–e** are a LOESS smoother (span=0.1) highlighting long-term trends. Black dashed lines in plots **a–c** represent modern mean values. The right side scales show the anomaly of the reconstructed values relative to modern mean values (in %). More contribution of summer rainfall ( $P_{JJA}$ ,  $P_{MJJAS}$ ) to annual rainfall indicates more seasonality (Yao et al. 2017b)

drylands to expand (Ding and Yu 1995; Ding et al. 2005; Li et al. 2014b). Second, the intensification of the EAWM and southward shift of the mid-latitude Westerlies prevent/delay the northward movement of the EASM airflows and therefore shorten the summer monsoon season and resultant rainfall amount (Ding and Yu 1995; Ding et al. 2005). Third, the melting of ice sheet alters ocean circulation, which then

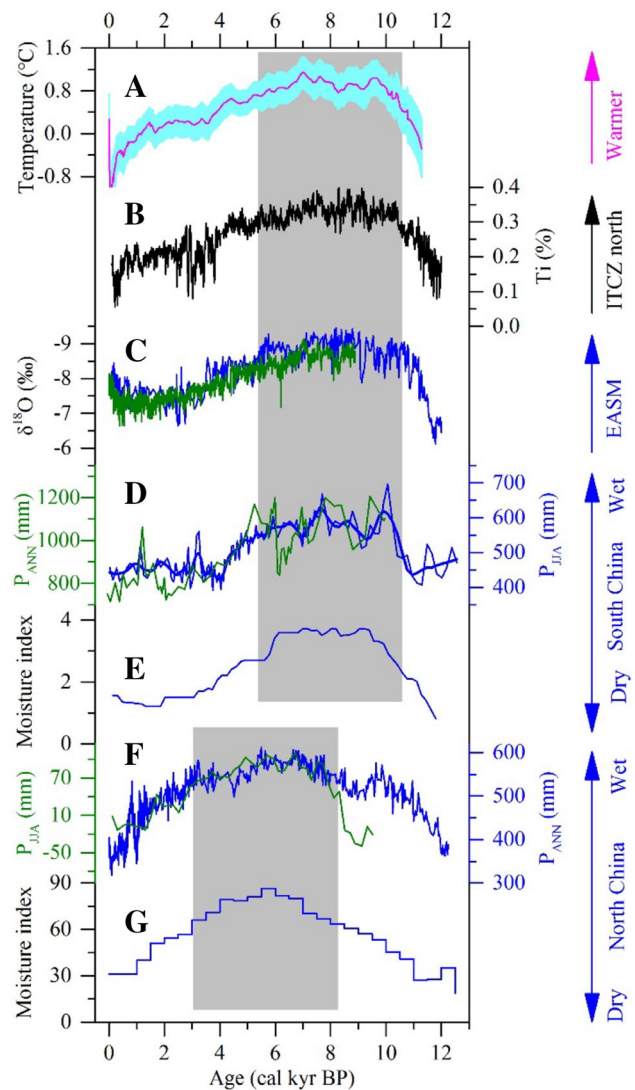


**Fig. 6** Comparison of inferred summer rainfall at Xinjie site with other Holocene records. **a** Temperature anomalies for extratropical Northern Hemisphere (Marcott et al. 2013). **b** Titanium concentration data from the Cariaco Basin, a proxy for the ITCZ (Haug et al. 2001). **c**  $\delta^{18}O$  records from Dongge Cave, a proxy for the EASM circulation (Dykoski et al. 2005; Wang et al. 2005). **d** Summer rainfall at Xinjie site (blue) and annual rainfall from Chaohu Lake (green) (Li et al. 2017b). **e** Synthesized moisture index for monsoonal South China (Zhao et al. 2009). **f** Annual rainfall from Gonghai Lake (blue) (Chen et al. 2015) and summer rainfall in semiarid North China (green) (Li et al. 2016). **g** Synthesized moisture index for arid/semiarid North China (Li et al. 2014b). The shaded area in plots **a–e** indicates an interval from ~10–6 cal kyr BP where maximum rainfall occurred in southern China. The shaded area in plots **f–g** indicates an interval from ~8–3 cal kyr BP where maximum rainfall occurred in northern China

affects atmospheric circulation (Chen et al. 2015; Sun et al. 2012). During the deglaciation, the Laurentide ice sheet experienced rapid melting and large volumes of freshwater were episodically released from Lake Agassiz into the North Atlantic Ocean (Fig. 8a) (Carlson et al. 2008; Teller

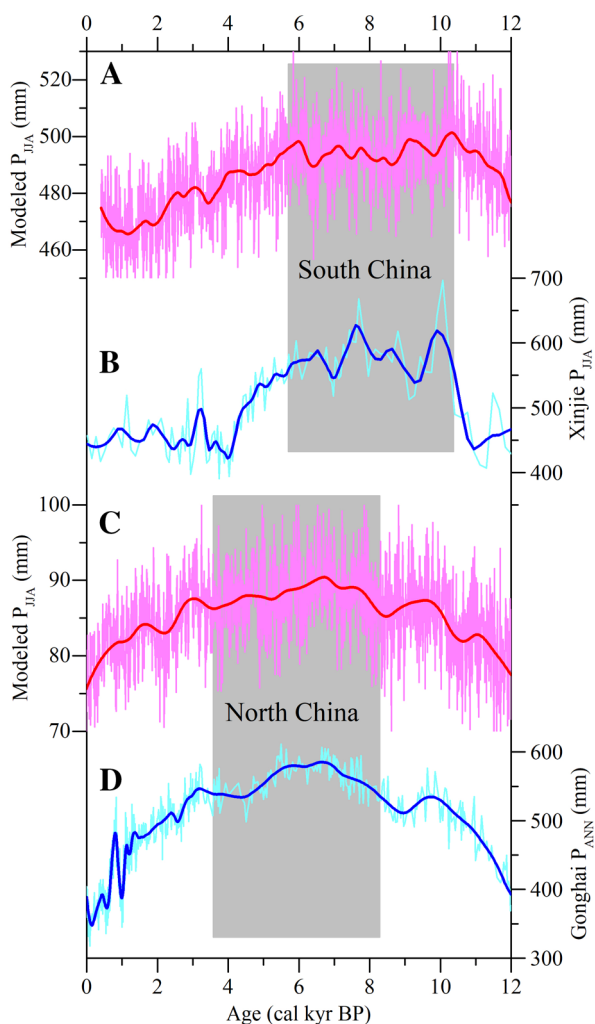


**Fig. 7** Different rainfall patterns between southern China (**b**) and northern China (**d**) during the Holocene and comparison with model results (**a**, **c**) from the full TraCE simulation (Liu et al. 2009). **a** Modeled summer precipitation in the region around Xinjie site. **b** Pollen-based summer precipitation reconstruction at Xinjie site in southern China. **c** Modeled summer precipitation in arid/semiarid northern China. **d** Pollen-based annual precipitation reconstruction at Gonghai Lake in northern China (Chen et al. 2015)

et al. 2002). The discharge of meltwater reduces sea surface salinity, thereby inhibiting the formation of North Atlantic Deep Water (NADW) and ultimately weakening the AMOC (Fig. 8b) and associated heat transport, which then causes anomalous cooling at high northern latitudes (Barber et al. 1999; Yu et al. 2010). The cooling of high northern latitudes alters interhemispheric thermal gradient and causes a southward shift in the mean position of the ITCZ (Chiang and Friedman 2012; Lu et al. 2013a; Schneider et al. 2014), thereby interrupting the insolation-driven trend of the EASM rainfall.

All the above processes might have influenced the EASM precipitation variability during the period from ~ 13

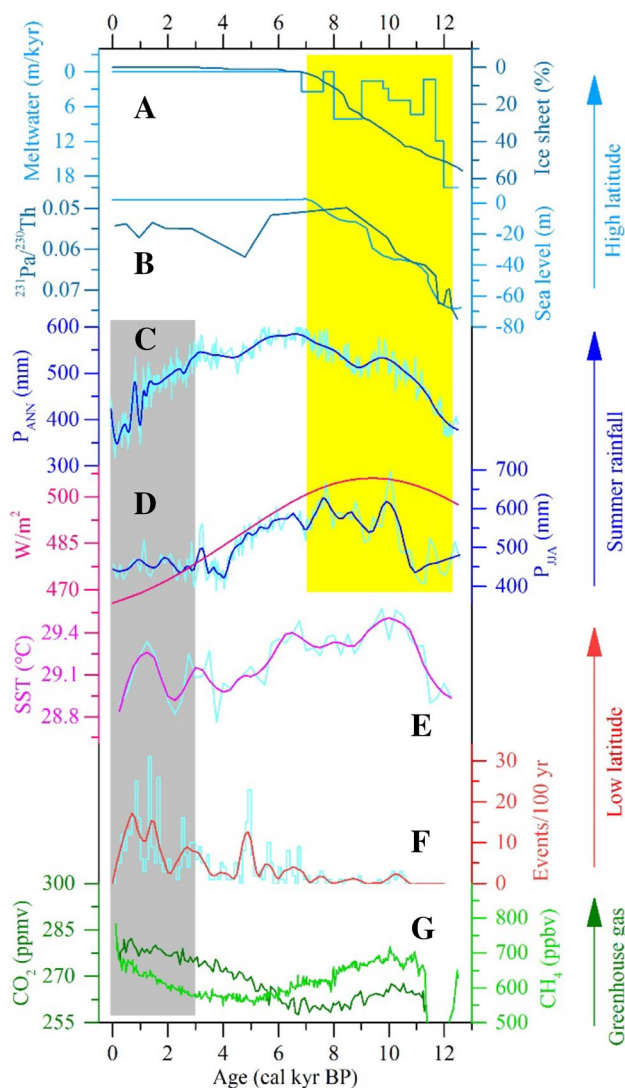


**Fig. 8** Comparison of summer rainfall records to various climate forcings. **a** Meltwater flux into the North Atlantic (Liu et al. 2014b) and Northern Hemisphere ice-sheet extent (Dyke 2004). **b**  $^{231}\text{Pa}/^{230}\text{Th}$  ratio in Bermuda, a proxy for the AMOC (McManus et al. 2004); and sea level change in the western Pacific (Liu et al. 2004). **c** Annual rainfall reconstruction from Gonghai Lake in northern China (Chen et al. 2015). **d** Summer rainfall reconstruction at Xinjie site together with  $65^\circ\text{N}$  July insolation (Laskar et al. 2004). **e** Sea-surface temperature (SST) reconstruction for the Indo-Pacific Warm Pool (Stott et al. 2004). **f** El Niño events per 100 years from Laguna Pallcacocha, southern Ecuador (Moy et al. 2002). **g** Atmospheric  $\text{CO}_2$  and  $\text{CH}_4$  concentrations from Dome Concordia, Antarctica (Louergue et al. 2008; Luthi et al. 2008). A LOESS smoother (span=0.1) was applied to highlight major trends in plots **c**–**f**. The yellow area in plots **a**–**d** indicates an interval from ~13–7 cal kyr BP where high-latitude forcing may influence the EASM precipitation. The grey area in plots **c**–**g** indicates an interval from ~3–0 cal kyr BP where ENSO and greenhouse gases may influence the EASM precipitation

to 7 cal kyr BP, which is supported by the single-forcing experiments of the TraCE-21 ka simulation (Fig. 10). Simulation MWF indicates reductions in summer precipitation

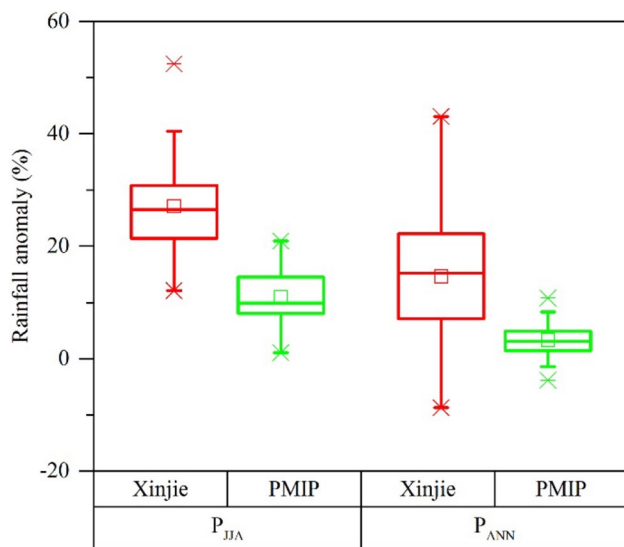


**Fig. 9** Comparison of mid-Holocene precipitation at Xinjie site to the PMIP model results. The red boxplots indicate pollen-based precipitation reconstructions at Xinjie site; while the green boxplots indicate simulated precipitation over China in 36 PMIP models (Jiang et al. 2013)

in both southern and northern China during the YD and 8.2-kyr events when a huge volume of meltwater was discharged into the North Atlantic Ocean (Fig. 10c). Although the performance of simulation ICE is not so good in simulating summer precipitation changes in the selected regions, it does show that autumn precipitation in northern China increased from ~13 to 7 cal kyr BP in response to the retreat of ice sheets (Fig. 10d). However, it should be noted that the response of East Asian summer precipitation to high-northern-latitude ice volume forcing during the early Holocene was spatially different. The summer precipitation in northern China was low during the early Holocene and did not reach a peak until ~6 cal kyr BP (Fig. 8c) (Chen et al. 2015; Li et al. 2014b; Lu et al. 2005, 2013a). In contrast, the summer precipitation in southern China has been high from ~10 cal kyr BP (Fig. 8d). The different rainfall response between southern and northern China to high latitude forcing is also supported by the TraCE-21 ka simulation. For example, the reduction of summer precipitation in northern China in the simulation MWF can be up to ~15%, whereas that of southern China is less than ~3%. This may be attributable to their different geographical locations and large-scale atmospheric circulations. As discussed in Sect. 4.3, the summer precipitation of southern China during the Holocene was mainly controlled by the EASM and ITCZ. When the ITCZ shifted northward rapidly after the YD and the EASM intensified (Dykoski et al. 2005; Haug et al. 2001), the summer rainfall of southern China increased in response. The arid/semiarid northern China, however, is located near or even outside the modern summer monsoon limit, where summer rainfall is

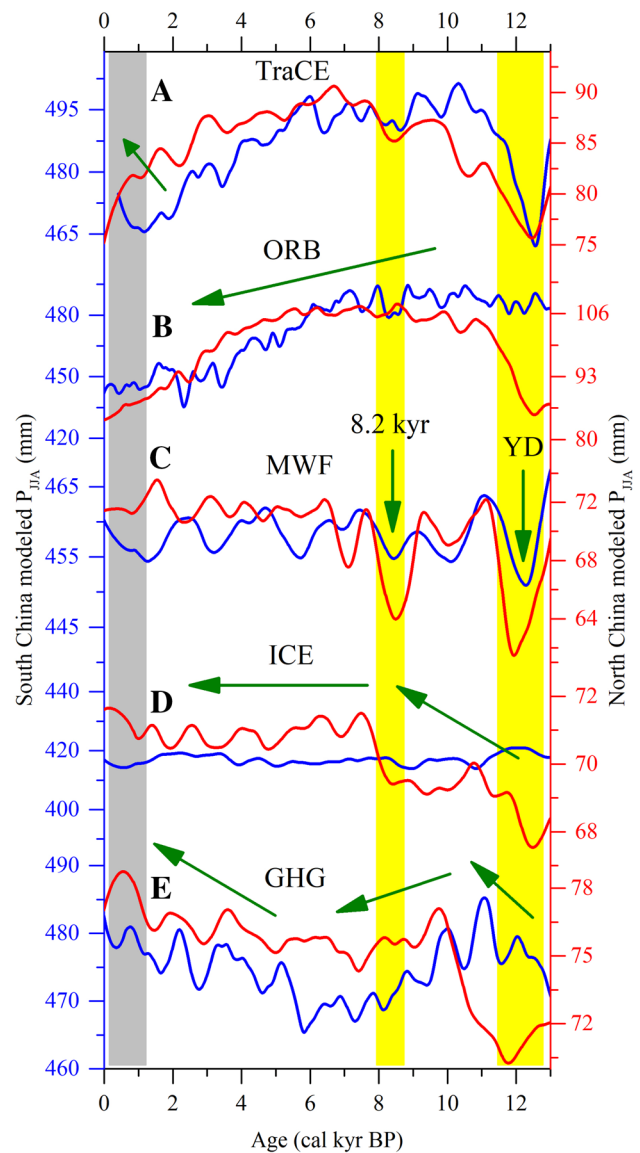


**Fig. 10** Modeled summer precipitation for southern China (blue) and northern China (red) in full and single forcing experiments from the TraCE-21 ka simulation (Liu et al. 2009). **a** Full TraCE simulation, with transient forcing changes in summer insolation, greenhouse gases, ice sheets and meltwater fluxes. **b** Only insolation forcing. **c** Only meltwater flux forcing. **d** Only ice sheet forcing. **e** Only greenhouse gas forcing. The yellow bars indicate intervals of low summer precipitation such as YD period and 8.2-kyr event, which were induced by meltwater flux forcing. The grey bar indicates the last millennium when summer precipitation in southern China increased partly due to greenhouse gas forcing. The green arrows indicate the trends of summer precipitation in full and single forcing experiments, respectively

influenced by multiple large-scale atmospheric circulations including the mid-latitude Westerlies as well as the EASM (Fig. 1) (An et al. 2012; Zhao and Yu 2012). The relatively strong Westerlies during the early Holocene may be responsible for the drier climate in northern China (Zhang et al.

2017), like the situation in central Asia (Chen et al. 2008). Besides, unlike southern China, which is located in the centre of the EASM influence, northern China is remote from the coastline and thus may be more sensitive to sea level fluctuations and resultant water vapour transport (Ding and Yu 1995). The lowering of sea level may also be accompanied by the southward retreat of summer monsoon boundary, which would substantially reduce the summer precipitation in northern China, thereby resulting in its arid/semiarid status (Ding et al. 2005).

#### 4.5.3 Low latitude forcing

Variability of sea-surface temperatures (SSTs) in the tropical Pacific and Indian Oceans has been proposed to influence the EASM circulation and associated rainfall on interannual to interdecadal timescales in the instrumental records (Chang et al. 2000; Ding et al. 2009; Yang and Lau 2004), whereas little is known about their linkage during the Holocene. Here we argue that the tropical SST changes may affect the spatial and temporal variability of EASM precipitation during the Holocene via two major intermediaries: (i) evaporation of seawater in the monsoon source that determines the amount of water vapour available for precipitation and (ii) the intensity of the WNP subtropical high that controls the position of the EASM rain belt.

First, since the water vapour supply for the EASM is mainly derived from the Indian Ocean and western tropical Pacific Ocean (Ding and Chan 2005; Drumond et al. 2011; Liu et al. 2015), variations in SSTs in these oceans are likely to have influenced the rate of evaporation and hence summer precipitation in East Asia during the Holocene. Our comparison shows that for the last ~ 13 kyr summer precipitation at Xinjie site always tracks changes in the sea surface temperatures of the Indo-Pacific Warm Pool (Fig. 8e) (Stott et al. 2004) and the tropical Indian Ocean (not shown) (Saraswat et al. 2013; Weldeab et al. 2014; Xu et al. 2008), supporting our assumption that SSTs and EASM rainfall were linked throughout the Holocene.

Second, ENSO-related SST changes affect the intensity of the WNP subtropical high and therefore the position of the EASM rain belt. Generally, a wet southern China is preceded by a warm (El Niño condition) equatorial eastern Pacific in the previous boreal winter (Chang et al. 2000). The convection associated with El Niño causes complementary cooling in the western North Pacific, which enhances the WNP subtropical high, thereby increasing the intensity and duration of summer precipitation in southern China while shortening the rainy season of northern China (Chang et al. 2000; Ding et al. 2009; Wang et al. 2000; Zhao et al. 2010). In addition, the enhancement and westward expansion of the WNP subtropical high can contribute to the coincident development of warm SST anomalies in northern Indian Ocean and South

China Sea (Chang et al. 2000). The warming of northern Indian Ocean and South China Sea will increase evaporation and hence supply more water vapour into the middle and lower reaches of the Yangtze River along the northwest flank of the WNP subtropical high, where the southwest monsoon wind is enhanced (Chang et al. 2000; Yang and Lau 2004). On the other hand, the anomalous strong WNP subtropical high and low-level southwesterly airflow can weaken the normal southeast monsoon wind over central and northern China, which consequently suppresses summer precipitation over semiarid northern China (Yang and Lau 2004; Zhao et al. 2010).

After ~6.8 cal kyr BP, the EASM precipitation responded more linearly to summer insolation forcing after the disappearance of glacial boundary conditions (Laskar et al. 2004). However, the contrary rainfall patterns between northern and southern China during the late Holocene cannot be explained by insolation forcing alone. We suppose that ENSO variability may have been responsible for this late Holocene anomaly. Both paleoclimate reconstructions (Moy et al. 2002) and model simulations (Liu et al. 2014a) indicate that El Niño events were most frequent during the late Holocene (Fig. 8f). The late Holocene El Niño might have led to southern floods and northern droughts during the late Holocene, as observed in instrumental records (Fig. 11) (Chang et al. 2000; Ding et al. 2009; Yang and Lau 2004). Our hypothesis is supported by speleothem magnetic mineral records from Heshang Cave in the middle Yangtze region, which show that ENSO-related storms and floods were strongest during the late Holocene (Zhu et al. 2017). The influence of ENSO on the intensity of the WNP subtropical high is also supported by a transient simulation using the Kiel Climate Model, which shows that the WNP subtropical high was relatively strong during the late Holocene (Jin et al. 2014; Wang et al. 2015). Consequently, the impact of ENSO forcing was superimposed on the effect of summer insolation forcing during the late Holocene, thereby causing opposite rainfall trends in southern and northern China at that time.

#### 4.5.4 Greenhouse gas forcing

Increases in atmospheric CO<sub>2</sub> concentration have been hypothesized as a potential driver of the EASM precipitation change on the Chinese Loess Plateau from the last glacial maximum (LGM) to the middle Holocene (Lu et al. 2013a). A large increase (~ 100 ppmv) in atmospheric CO<sub>2</sub> concentration from glacial state (LGM) to interglacial state (Holocene) would dramatically warm up high northern latitudes (Liu et al. 2009, 2012), which leads to a northward migration of the ITCZ and therefore the EASM rain belt (Chiang and Friedman 2012; Lu et al. 2013a; Schneider et al. 2014). Temperature reconstructions and transient simulations indicate that the global warming during the last

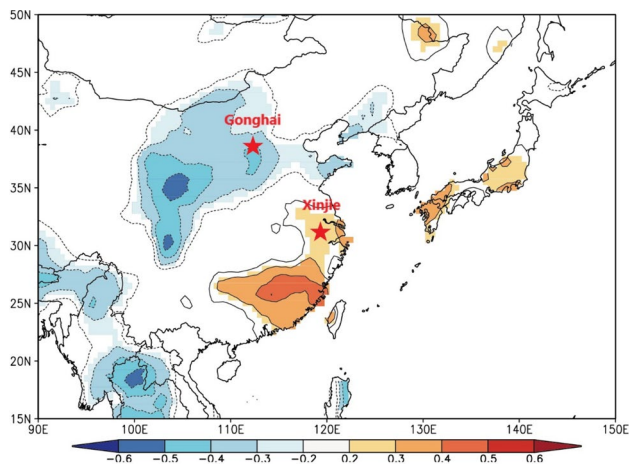


**Fig. 11** Correlation map for Niño3 relative index with CRUTS4.0 gridded ( $0.5^\circ \times 0.5^\circ$ ) precipitation fields during the period 1960–2014 (Harris et al. 2014). Colored contours represent significant correlation coefficients ( $p < 10\%$ )

deglaciation was preceded by increasing  $\text{CO}_2$  concentration (Shakun et al. 2012). Sensitivity experiments further show that the Bølling-Allerød warming was dominated by the  $\text{CO}_2$  forcing (Liu et al. 2009), with polar amplification of attendant cryosphere feedbacks (Liu et al. 2012). During the Holocene, however, the change in  $\text{CO}_2$  concentration is small ( $\sim 20$  ppmv), and whether it can influence the EASM precipitation remains unclear. During the early and middle Holocene when summer precipitation at Xinjie site was high,  $\text{CO}_2$  concentration was low and increased steadily from  $\sim 8$  cal kyr BP to the late Holocene (Fig. 8g), suggesting that  $\text{CO}_2$  forcing may not be the major driving force of the EASM precipitation variability during the Holocene. If it has been a major driver, the summer precipitation should have increased from the early to late Holocene. The maximum values of  $\text{CO}_2$  in the late Holocene may, however, have contributed to the anomalous increase of summer precipitation at Xinjie site since  $\sim 2$  cal kyr BP. The lowering of summer insolation tends to reduce the amount of summer precipitation (Kutzbach et al. 2008), while an increase in the  $\text{CO}_2$  concentration tends to enhance summer rainfall (Lu et al. 2013a) (Fig. 10b, e). We argue that the  $\text{CO}_2$  forcing may have offset the effect of insolation forcing during the late Holocene when summer insolation forcing was weak. In addition, there may be a threshold for  $\text{CO}_2$  forcing to overcome summer insolation forcing. For example,  $\text{CO}_2$  concentrations greater than  $\sim 277$  ppmv at  $\sim 2$  cal kyr BP may have forced the upward trend of summer precipitation at Xinjie site. Our hypothesis of  $\text{CO}_2$  forcing on the Holocene EASM precipitation is supported by the GHG single forcing experiment (Fig. 10e), indicating that summer precipitation in both southern and northern China began to increase from  $\sim 7$  cal kyr BP. A detail comparison between the GHG and

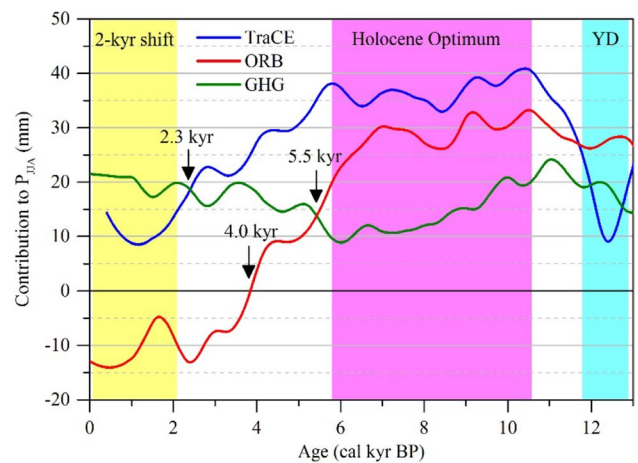


**Fig. 12** Absolute contributions of greenhouse gas forcing and summer insolation forcing to the Holocene summer precipitation in the region around Xinjie site simulated in the TraCE experiments (Liu et al. 2009). Arrows indicate that GHG overcame ORB at  $\sim 5.5$  cal kyr BP, and greenhouse gas forcing became the major and/or even the only positive contributor for the late Holocene summer precipitation since  $\sim 2.3$  cal kyr BP. Another arrow indicates that summer insolation has a negative contribution to summer precipitation since  $\sim 4.0$  cal kyr BP

ORB simulations (Fig. 12) indicates that greenhouse gas forcing exceeded summer insolation forcing at  $\sim 5.5$  cal kyr BP and then became the major contributor for late Holocene summer rainfall. After  $\sim 2.3$  cal kyr BP, greenhouse gas forcing exceeded full forcing and thus was the greatest and even the only positive contributor for summer precipitation. Besides, greenhouse gas forcing has a persistent positive contribution to summer rainfall during the whole Holocene, while summer insolation forcing has a negative contribution since  $\sim 4.0$  cal kyr BP (Fig. 12). Obviously, it is the greenhouse gas forcing that offset summer insolation forcing and thereby kept summer precipitation in the region around Xinjie site to be positive in the late Holocene (Fig. 12). Summer insolation forcing alone would lead the late Holocene climate to be drier than that during the LGM. In contrast, greenhouse gas forcing alone is sufficient to explain the higher summer precipitation during the late Holocene than during the LGM (Fig. 12). An increase in  $\text{CO}_2$  concentration would also enhance sea-surface temperatures, which in turn affect summer monsoon precipitation (Hu et al. 2000). The strengthening of ENSO throughout the Holocene (Moy et al. 2002) was accompanied by a gradual increase in  $\text{CO}_2$  concentrations, indicating a possible causal linkage between them. Similarly,  $\text{CH}_4$  concentrations may have had a similar effect on the EASM precipitation (Fig. 8g). Therefore, the late Holocene summer rainfall anomaly at Xinjie site in southern China (the 2-kyr shift) might be largely attributable to greenhouse gas forcing. Overall, summer insolation and greenhouse gases are the two most important contributor to



Holocene summer precipitation in the EASM core region, with summer insolation playing a major role during the early and middle Holocene and greenhouse gases playing a major role during the late Holocene.

## 5 Conclusions

We have presented high-resolution and pollen-based quantitative reconstructions of both annual and summer precipitation covering the last 12.5 kyr for the lower Yangtze region. This is the first quantitative reconstruction of Holocene summer precipitation for tropical and subtropical China. Our summer precipitation reconstruction is consistent with paleoclimate records from tropical and subtropical China, indicating ~30% higher summer monsoon rainfall during the early and middle Holocene at ~10–6 cal kyr BP; but distinct from those in arid/semiarid northern China that indicate a mid-Holocene rainfall maximum at ~8–3 cal kyr BP. Our reconstructions also suggest that the precipitation was less seasonal in warm and wet periods but more seasonal in cold and dry periods. Our investigation of the underlying forcing mechanisms indicates that summer precipitation in arid/semiarid northern China was strongly affected by high-northern-latitude ice volume during the early Holocene despite high summer insolation. In contrast, summer rainfall in southern China was mainly controlled by summer insolation forcing. However, over the last two millennia the rainfall has deviated from the downward trend of summer insolation. We argue that CO<sub>2</sub> forcing might have overcome summer insolation forcing and contributed to the late Holocene rainfall anomaly at Xinjie site as well as “the 2-kyr shift” in cave records (Cheng et al. 2016). The TraCE-21 ka transient simulation supports that greenhouse gas forcing exceeded summer insolation forcing at ~5.5 cal kyr BP and then became the major contributor for late Holocene summer rainfall, especially since ~2.3 cal kyr BP. Besides, tropical sea-surface temperatures could modulate the EASM precipitation by affecting evaporation of seawater in the monsoon source. Furthermore, we attribute the rapid drying of northern China and anomalous wetting of southern China during the late Holocene to the influence of El Niño/Southern Oscillation. The different rainfall patterns and responses between southern China and arid/semiarid northern China indicate the complex rainfall structure of the subtropical EASM during the Holocene, which are very helpful for predicting future precipitation changes in China in the scenario of global warming. Moreover, comparisons of quantitative reconstructions to model results suggest that the PMIP simulations underestimate the magnitude of Holocene precipitation changes. Therefore, quantitative rainfall reconstructions are essential for calibration of paleoclimate models.

Our discussions about the variability and forcing mechanisms of the EASM precipitation are based on quantitative reconstructions that are independent of speleothem  $\delta^{18}\text{O}$  records whose interpretation remains controversial and therefore draw a more unambiguous conclusion. However, quantitative records of Holocene summer precipitation are still insufficient. We therefore strongly recommend that additional quantitative reconstructions of summer precipitation should be made in the future to provide a more detailed picture of the spatial and temporal variability of the EASM precipitation during the Holocene. We also recommend that additional transient simulations and sensitivity experiments with high spatial resolution and calibrated by quantitative records should be performed to identify the individual and combined effects of insolation, ice volume, freshwater flux, sea-surface temperatures and greenhouse gas concentrations on the spatial and temporal variability of the EASM precipitation during the Holocene.

**Acknowledgements** We are grateful to Prof. Fahu Chen for inspiring us to write this paper, to Prof. Zhuo Zheng, Qinghai Xu, and Houyuan Lu for providing the modern surface pollen data, to three anonymous reviewers for their helpful comments that greatly improved this manuscript. We thank all members of the East Asian Pollen Database (EAPD) and Chinese Quaternary Pollen Database (CPD) for their dedication. This research is supported by National Key R&D Program of China (2016YFA0600501), National Natural Science Foundation of China (41571179 and 41671196) and Science & Technology Support Program of Jiangsu Province, China (BE2014705).

## References

- An Z (2000) The history and variability of the East Asian paleomonsoon climate. *Quat Sci Rev* 19:171–187. [https://doi.org/10.1016/S0277-3791\(99\)00060-8](https://doi.org/10.1016/S0277-3791(99)00060-8)
- An Z et al (2000) Asynchronous Holocene optimum of the East Asian monsoon. *Quat Sci Rev* 19:743–762. [https://doi.org/10.1016/S0277-3791\(99\)00031-1](https://doi.org/10.1016/S0277-3791(99)00031-1)
- An Z et al (2012) Interplay between the Westerlies and Asian monsoon recorded in Lake Qinghai sediments since 32 ka. *Sci Rep* 2:619. <https://doi.org/10.1038/srep00619>
- An Z et al (2015) Global monsoon dynamics and climate change. *Annu Rev Earth Planet Sci* 43:29–77. <https://doi.org/10.1146/annurev-earth-060313-054623>
- Barber DC et al (1999) Forcing of the cold event of 8,200 years ago by catastrophic drainage of Laurentide lakes. *Nature* 400:344–348
- Berger A (1978) Long-term variations of daily insolation and quaternary climatic changes. *J Atmos Sci* 35:2362–2367 [https://doi.org/10.1175/1520-0469\(1978\)035<2362:ltvodi>2.0.co;2](https://doi.org/10.1175/1520-0469(1978)035<2362:ltvodi>2.0.co;2)
- Birks H (1998) Numerical tools in palaeolimnology—progress, potentialities, and problems. *J Paleolimnol* 20:307–332
- Birks HJB (2003) Quantitative palaeoenvironmental reconstructions from Holocene biological data. In: Mackay A, Battarbee RW, Birks HJB, Oldfield F (eds) *Global change in the Holocene*. Hodder Arnold, London, pp 107–123
- Bond G et al (1997) A pervasive millennial-scale cycle in North Atlantic Holocene and Glacial. *Clim Sci* 278:1257–1266. <https://doi.org/10.1126/science.278.5341.1257>

- Bond G et al (2001) Persistent solar influence on North Atlantic climate during the Holocene. *Science* 294:2130–2136. <https://doi.org/10.1126/science.1065680>
- Cao X, Xu Q, Jing Z, Tang J, Li Y, Tian F (2010) Holocene climate change and human impacts implied from the pollen records in Anyang central China. *Quat Int* 227:3–9. <https://doi.org/10.1016/j.quaint.2010.03.019>
- Cao X-Y, Herzschuh U, Telford RJ, Ni J (2014) A modern pollen–climate dataset from China and Mongolia: assessing its potential for climate reconstruction. *Rev Palaeobot Palynol* 211:87–96. <https://doi.org/10.1016/j.revpalbo.2014.08.007>
- Carlson AE (2013) PALEOCLIMATE I the younger dryas climate event A2—Elias, Scott A. In: Mock CJ (ed) *Encyclopedia of quaternary science*, 2nd edn. Elsevier, Amsterdam, pp 126–134. <https://doi.org/10.1016/B978-0-444-53643-3.00029-7>
- Carlson AE et al (2008) Rapid early Holocene deglaciation of the Laurentide ice sheet. *Nat Geosci* 1:620–624
- CASS (1992) Radiocarbon dates in Chinese archaeology. Cultural Relics Publishing House, Beijing
- Chang C-P, Zhang Y, Li T (2000) Interannual and interdecadal variations of the East Asian Summer Monsoon and Tropical Pacific SSTs. Part I: roles of the subtropical ridge. *J Clim* 13:4310–4325. [https://doi.org/10.1175/1520-0442\(2000\)013<4310:iaivot>2.0.co;2](https://doi.org/10.1175/1520-0442(2000)013<4310:iaivot>2.0.co;2)
- Chen MT, Huang CY (1998) Ice-volume forcing of winter monsoon climate in the South China Sea. *Paleoceanography* 13:622–633. <https://doi.org/10.1029/98PA02356>
- Chen F et al (2008) Holocene moisture evolution in arid central Asia and its out-of-phase relationship with Asian monsoon history. *Quat Sci Rev* 27:351–364. <https://doi.org/10.1016/j.quascirev.2007.10.017>
- Chen W, Wang W-M, Dai X-R (2009) Holocene vegetation history with implications of human impact in the Lake Chaohu area, Anhui Province East China. *Veg Hist Archaeobot* 18:137–146. <https://doi.org/10.1007/s00334-008-0173-7>
- Chen F et al (2014) Holocene vegetation history, precipitation changes and Indian Summer Monsoon evolution documented from sediments of Xingyun Lake, south-west China. *J Quat Sci* 29:661–674. <https://doi.org/10.1002/jqs.2735>
- Chen F et al (2015) East Asian summer monsoon precipitation variability since the last deglaciation. *Sci Rep* 5:11186. <https://doi.org/10.1038/srep11186>
- Cheng H, Sinha A, Wang X, Cruz FW, Edwards RL (2012) The Global Paleomonsoon as seen through speleothem records from Asia and the Americas. *Clim Dyn* 39:1045–1062. <https://doi.org/10.1007/s00382-012-1363-7>
- Cheng H et al (2016) The Asian monsoon over the past 640,000 years and ice age terminations. *Nature* 534:640–646. <https://doi.org/10.1038/nature18591>
- Chiang JCH, Friedman AR (2012) Extratropical cooling, interhemispheric thermal gradients, and tropical climate change. *Annu Rev Earth Planet Sci* 40:383–412 doi. <https://doi.org/10.1146/annurev-earth-042711-105545>
- Collins WD et al (2006) The community climate system model version 3 (CCSM3). *J Clim* 19:2122–2143. <https://doi.org/10.1175/jcli3761.1>
- Dearing JA et al (2008) Using multiple archives to understand past and present climate–human–environment interactions: the lake Erhai catchment, Yunnan Province China. *J Paleolimnol* 40:3–31. <https://doi.org/10.1007/s10933-007-9182-2>
- Ding Y, Chan JCL (2005) The East Asian summer monsoon: an overview. *Meteorol Atmos Phys* 89:117–142. <https://doi.org/10.1007/s00703-005-0125-z>
- Ding Z, Yu Z (1995) Forcing mechanisms of paleomonsoons over East Asia. *Quat Sci (in Chin)* 1:63–74
- Ding Z, Liu T, Rutter NW, Yu Z, Guo Z, Zhu R (1995) Ice-volume forcing of East Asian winter monsoon variations in the past 800,000 Years. *Quat Res* 44:149–159. <https://doi.org/10.1006/qres.1995.1059>
- Ding ZL, Derbyshire E, Yang SL, Yu ZW, Xiong SF, Liu TS (2002) Stacked 2.6-Ma grain size record from the Chinese loess based on five sections and correlation with the deep-sea  $\delta^{18}O$  record. *Paleoceanography*. <https://doi.org/10.1029/2001PA000725>
- Ding ZL, Derbyshire E, Yang SL, Sun JM, Liu TS (2005) Stepwise expansion of desert environment across northern China in the past 3.5 Ma and implications for monsoon evolution. *Earth Planet Sci Lett* 237:45–55. <https://doi.org/10.1016/j.epsl.2005.06.036>
- Ding Y, Wang Z, Sun Y (2008) Inter-decadal variation of the summer precipitation in East China and its association with decreasing Asian summer monsoon. Part I: observed evidences International. *J Climatol* 28:1139–1161. <https://doi.org/10.1002/joc.1615>
- Ding Y, Sun Y, Wang Z, Zhu Y, Song Y (2009) Inter-decadal variation of the summer precipitation in China and its association with decreasing Asian summer monsoon Part II: possible causes International. *J Climatol* 29:1926–1944. <https://doi.org/10.1002/joc.1759>
- Dong J et al (2010) A high-resolution stalagmite record of the Holocene East Asian monsoon from Mt Shennongjia central China. *Holocene* 20:257–264. <https://doi.org/10.1177/0959683609350393>
- Drumond A, Nieto R, Gimeno L (2011) Sources of moisture for China and their variations during drier and wetter conditions in 2000–2004: a Lagrangian approach. *Clim Res* 50:215–225
- Dyke AS (2004) An outline of North American deglaciation with emphasis on central and northern Canada. *Dev Quat Sci* 2:373–424. [https://doi.org/10.1016/S1571-0866\(04\)80209-4](https://doi.org/10.1016/S1571-0866(04)80209-4)
- Dykoski CA et al (2005) A high-resolution, absolute-dated Holocene and deglacial Asian monsoon record from Dongge Cave, China. *Earth Planet Sci Lett* 233:71–86. <https://doi.org/10.1016/j.epsl.2005.01.036>
- Fægri K, Iversen J (1989) A textbook of pollen analysis. *J Biogeogr* 14:328
- Fick SE, Hijmans RJ (2017) WorldClim 2: new 1-km spatial resolution climate surfaces for global land areas. *Int J Climatol*. <https://doi.org/10.1002/joc.5086>
- Fleitmann D, Mudelsee M, Burns SJ, Bradley RS, Kramers J, Matter A (2008) Evidence for a widespread climatic anomaly at around 9.2 ka before present. *Paleoceanography*. <https://doi.org/10.1029/2007PA001519>
- Grimm EC (1987) CONISS: a FORTRAN 77 program for stratigraphically constrained cluster analysis by the method of incremental sum of squares ☆. *Comput Geosci* 13:13–35
- Grimm EC, Maher LJ, Nelson DM (2009) The magnitude of error in conventional bulk-sediment radiocarbon dates from central North America. *Quat Res* 72:301–308. <https://doi.org/10.1016/j.yqres.2009.05.006>
- Hao Q et al (2012) Delayed build-up of Arctic ice sheets during 400,000-year minima in insolation variability. *Nature* 490:393–396. <https://doi.org/10.1038/nature11493>
- Harris I, Jones PD, Osborn TJ, Lister DH (2014) Updated high-resolution grids of monthly climatic observations—the CRU TS3.10 dataset. *Int J Climatol* 34:623–642. <https://doi.org/10.1002/joc.3711>
- Haug GH, Hughen KA, Sigman DM, Peterson LC, Röhl U (2001) Southward migration of the intertropical convergence zone through the Holocene. *Science* 293:1304–1308. <https://doi.org/10.1126/science.1059725>
- He F, Shakun JD, Clark PU, Carlson AE, Liu Z, Otto-Bliesner BL, Kutzbach JE (2013) Northern Hemisphere forcing of Southern

- Hemisphere climate during the last deglaciation. *Nature* 494:81. <https://doi.org/10.1038/nature11822>
- Hill MO, Gauch HG (1980) Detrended correspondence analysis: an improved ordination technique. *Vegetation* 42:47–58. <https://doi.org/10.1007/bf00048870>
- Hu ZZ, Latif M, Roeckner E, Bengtsson L (2000) Intensified Asian Summer Monsoon and its variability in a coupled model forced by increasing greenhouse gas concentrations. *Geophys Res Lett* 27:2681–2684. <https://doi.org/10.1029/2000GL011550>
- Hu C, Henderson GM, Huang J, Xie S, Sun Y, Johnson KR (2008) Quantification of Holocene Asian monsoon rainfall from spatially separated cave records. *Earth Planet Sci Lett* 266:221–232. <https://doi.org/10.1016/j.epsl.2007.10.015>
- Innes JB, Zong Y, Wang Z, Chen Z (2014) Climatic and palaeoecological changes during the mid- to Late Holocene transition in eastern China: high-resolution pollen and non-pollen palynomorph analysis at Pingwang, Yangtze coastal lowlands. *Quat Sci Rev* 99:164–175. <https://doi.org/10.1016/j.quascirev.2014.06.013>
- Jiang W et al (2006) Reconstruction of climate and vegetation changes of Lake Bayanchagan (Inner Mongolia): Holocene variability of the East Asian monsoon. *Quat Res* 65:411–420. <https://doi.org/10.1016/j.yqres.2005.10.007>
- Jiang D, Tian Z, Lang X (2013) Mid-Holocene net precipitation changes over China: model–data comparison. *Quat Sci Rev* 82:104–120. <https://doi.org/10.1016/j.quascirev.2013.10.017>
- Jin L, Schneider B, Park W, Latif M, Khon V, Zhang X (2014) The spatial–temporal patterns of Asian summer monsoon precipitation in response to Holocene insolation change: a model–data synthesis. *Quat Sci Rev* 85:47–62. <https://doi.org/10.1016/j.quascirev.2013.11.004>
- Johnsen SJ et al (2001) Oxygen isotope and palaeotemperature records from six Greenland ice-core stations: Camp Century, Dye-3, GRIP, GISP2, Renland and NorthGRIP. *J Quat Sci* 16:299–307. <https://doi.org/10.1002/jqs.622>
- Joos F, Spahni R (2008) Rates of change in natural and anthropogenic radiative forcing over the past 20,000 years. *Proc Natl Acad Sci USA* 105:1425
- Joussaume S, Taylor K (1995) Status of the paleoclimate modelling intercomparison project (PMIP). In: Gates WL (ed) Proceedings of the first international AMIP conference. World Meteorol Organ, Geneva, pp 425–430
- Juggins S, Birks HJB (2012) Quantitative environmental reconstructions from biological data. In: Birks HJB, Lotter AF, Juggins S, Smol JP (eds) Tracking environmental change using Lake Sediments: data handling and numerical techniques. Springer, Dordrecht, pp 431–494. [https://doi.org/10.1007/978-94-007-2745-8\\_14](https://doi.org/10.1007/978-94-007-2745-8_14)
- Juggins S, Telford RJ (2012) Exploratory data analysis and data display. In: Birks HJB, Lotter AF, Juggins S, Smol JP (eds) Tracking environmental change using Lake Sediments: data handling and numerical techniques. Springer, Dordrecht, pp 123–141. [https://doi.org/10.1007/978-94-007-2745-8\\_5](https://doi.org/10.1007/978-94-007-2745-8_5)
- Kanamitsu M, Ebisuzaki W, Woollen J, Yang S-K, Hnilo JJ, Fiorino M, Potter GL (2002) NCEP–DOE AMIP-II reanalysis (R-2). *Bull Am Meteorol Soc* 83:1631–1643. <https://doi.org/10.1175/BAMS-83-11-1631>
- Kramer A, Herzschuh U, Mischke S, Zhang C (2010) Holocene tree-line shifts and monsoon variability in the Hengduan Mountains (southeastern Tibetan Plateau), implications from palynological investigations. *Palaeogeogr Palaeoclimatol Palaeoecol* 286:23–41. <https://doi.org/10.1016/j.palaeo.2009.12.001>
- Kutzbach JE (1981) Monsoon climate of the early Holocene: climate experiment with the earth's orbital parameters for 9000 years ago. *Science* 214:59–61. <https://doi.org/10.1126/science.214.4516.59>
- Kutzbach JE, Guetter PJ (1986) The influence of changing orbital parameters and surface boundary conditions on climate simulations for the Past 18,000 Years. *J Atmos Sci* 43:1726–1759. [https://doi.org/10.1175/1520-0469\(1986\)043<1726:tio cop>2.0.co;2](https://doi.org/10.1175/1520-0469(1986)043<1726:tio cop>2.0.co;2)
- Kutzbach JE, Liu X, Liu Z, Chen G (2008) Simulation of the evolutionary response of global summer monsoons to orbital forcing over the past 280,000 years. *Clim Dyn* 30:567–579. <https://doi.org/10.1007/s00382-007-0308-z>
- Laskar J, Robutel P, Joutel F, Gastineau M, Correia A, Levrard B (2004) A long-term numerical solution for the insolation quantities of the Earth. *Astron Astrophys* 428:261–285
- LeGrande AN, Schmidt GA (2009) Sources of Holocene variability of oxygen isotopes in paleoclimate archives. *Clim Past* 5:441–455. <https://doi.org/10.5194/cp-5-441-2009>
- Li L (2011) Research on the missing causes of the archaeological sites in Early Holocene in Taihu Lake area, Jiangsu Province. PhD, Nanjing University
- Li L, Zhu C, Lin L, Zhao Q, Shi G, Zheng C, Fan C (2009) Evidence for marine transgression between 7500–5400BC at the Luotudun Site in Yixing, Jiangsu Province. *J Geogr Sci* 19:671–680. <https://doi.org/10.1007/s11442-009-0671-2>
- Li J, Wu Z, Jiang Z, He J (2010) Can global warming strengthen the East Asian summer monsoon? *J Clim* 23:6696–6705. <https://doi.org/10.1175/2010jcli3434.1>
- Li J et al (2014a) Human influence as a potential source of bias in pollen-based quantitative climate reconstructions. *Quat Sci Rev* 99:112–121
- Li Q, Wu H, Yu Y, Sun A, Marković SB, Guo Z (2014b) Reconstructed moisture evolution of the deserts in northern China since the Last Glacial Maximum and its implications for the East Asian summer monsoon. *Global Planet Chang* 121:101–112. <https://doi.org/10.1016/j.gloplacha.2014.07.009>
- Li J et al (2015) Assessing the importance of climate variables for the spatial distribution of modern pollen data in China. *Quat Res* 83:287–297. <https://doi.org/10.1016/j.yqres.2014.12.002>
- Li J et al (2016) East Asian summer monsoon precipitation variations in China over the last 9500 years: a comparison of pollen-based reconstructions and model simulations. *Holocene* 26:592–602. <https://doi.org/10.1177/0959683615612564>
- Li J et al (2017a) Quantitative precipitation estimates for the north-eastern Qinghai-Tibetan Plateau over the last 18,000 years. *J Geophys Res Atmos*. <https://doi.org/10.1002/2016JD026333>
- Li J et al (2017b) Quantitative Holocene climatic reconstructions for the lower Yangtze region of China. *Clim Dyn*. <https://doi.org/10.1007/s00382-017-3664-3>
- Li J et al (2017c) Quantifying climatic variability in monsoonal northern China over the last 2200 years and its role in driving Chinese dynastic changes. *Quat Sci Rev* 159:35–46. <https://doi.org/10.1016/j.quascirev.2017.01.009>
- Liu T, Ding Z (1992) Stepwise coupled process of monsoon circulation and variation of continental ice volume over the last 2.5 Ma. *Quat Sci* 12(1):12–23 (in Chinese with English abstract)
- Liu K-B, Sun S, Jiang X (1992) Environmental change in the Yangtze River delta since 12,000 years BP. *Quat Res* 38:32–45. [https://doi.org/10.1016/0033-5894\(92\)90028-H](https://doi.org/10.1016/0033-5894(92)90028-H)
- Liu JP, Milliman JD, Gao S, Cheng P (2004) Holocene development of the Yellow River's subaqueous delta North Yellow Sea. *Mar Geol* 209:45–67. <https://doi.org/10.1016/j.margeo.2004.06.009>
- Liu Z et al (2009) Transient simulation of Last Deglaciation with a new mechanism for Bølling–Allerød warming. *Science* 325:310–314. <https://doi.org/10.1126/science.1171041>
- Liu Z et al (2012) Younger Dryas cooling and the Greenland climate response to CO<sub>2</sub>. *Proc Natl Acad Sci* 109:11101–11104 <https://doi.org/10.1073/pnas.1202183109>
- Liu Z, Lu Z, Wen X, Otto-Bliesner BL, Timmermann A, Cobb KM (2014a) Evolution and forcing mechanisms of El Niño

- over the past 21,000 years. *Nature* 515:550–553. <https://doi.org/10.1038/nature13963>
- Liu Z et al (2014b) Chinese cave records and the East Asia Summer Monsoon. *Quat Sci Rev* 83:115–128. <https://doi.org/10.1016/j.quascirev.2013.10.021>
- Liu J, Chen J, Zhang X, Li Y, Rao Z, Chen F (2015) Holocene East Asian summer monsoon records in northern China and their inconsistency with Chinese stalagmite  $\delta^{18}O$  records. *Earth Sci Rev* 148:194–208. <https://doi.org/10.1016/j.earscirev.2015.06.004>
- Loulergue L et al (2008) Orbital and millennial-scale features of atmospheric  $CH_4$  over the past 800,000 years. *Nature* 453:383–386. <https://doi.org/10.1038/nature06950>
- Lu H, Zhang F, Liu X, Duce RA (2004) Periodicities of palaeoclimatic variations recorded by loess-paleosol sequences in China. *Quat Sci Rev* 23:1891–1900. <https://doi.org/10.1016/j.quascirev.2004.06.005>
- Lu H et al (2005) Late Quaternary aeolian activity in the Mu Us and Otindag dune fields (north China) and lagged response to insolation forcing. *Geophys Res Lett*. <https://doi.org/10.1029/2005GL024560>
- Lu H et al (2011a) Modern pollen distributions in Qinghai–Tibetan Plateau and the development of transfer functions for reconstructing Holocene environmental changes. *Quat Sci Rev* 30:947–966. <https://doi.org/10.1016/j.quascirev.2011.01.008>
- Lu H et al (2011b) Holocene climatic changes revealed by aeolian deposits from the Qinghai Lake area (northeastern Qinghai–Tibetan Plateau) and possible forcing mechanisms. *Holocene* 21:297–304
- Lu H et al (2013a) Variation of East Asian monsoon precipitation during the past 21 k.y. and potential  $CO_2$  forcing. *Geology* 41:1023–1026. <https://doi.org/10.1130/g34488.1>
- Lu H et al (2013b) Chinese deserts and sand fields in Last Glacial maximum and Holocene optimum. *Chin Sci Bull* 58:2775–2783
- Lu F, Zhu C, Ma C, Zhang W, Li B, Li K (2015) High-resolution palynological record in the western region of Taihu Lake since 8.2 ka BP. *J Stratigr* 39:116–123
- Luthi D et al (2008) High-resolution carbon dioxide concentration record 650,000–800,000 years before present. *Nature* 453:379–382. <https://doi.org/10.1038/nature06949>
- Ma C et al (2008) High-resolution geochemistry records of climate changes since late-glacial from Dajiuhe peat in Shennongjia Mountains, Central China. *Chin Sci Bull* 53:28–41. <https://doi.org/10.1007/s11434-008-5007-6>
- Ma C, Zhu C, Zheng C, Yin Q, Zhao Z (2009) Climate changes in East China since the Late-glacial inferred from high-resolution mountain peat humification records. *Sci Chin Ser D Earth Sci* 52:118–131. <https://doi.org/10.1007/s11430-009-0003-5>
- Maher BA, Thompson R (2012) Oxygen isotopes from Chinese caves: records not of monsoon rainfall but of circulation regime. *J Quat Sci* 27:615–624. <https://doi.org/10.1002/jqs.2553>
- Manly BF (2006) Randomization, bootstrap and Monte Carlo methods in biology. CRC Press, Boca Raton
- Marcott SA, Shakun JD, Clark PU, Mix AC (2013) A reconstruction of regional and global temperature for the past 11,300 years. *Science* 339:1198–1201. <https://doi.org/10.1126/science.1228026>
- McManus JF, Francois R, Gherardi JM, Keigwin LD, Brown-Leger S (2004) Collapse and rapid resumption of Atlantic meridional circulation linked to deglacial climate changes. *Nature* 428:834–837. <https://doi.org/10.1038/nature02494>
- Moy CM, Seltzer GO, Rodbell DT, Anderson DM (2002) Variability of El Niño/Southern Oscillation activity at millennial timescales during the Holocene epoch. *Nature* 420:162–165
- Okuda M et al (2003) Late Holocene vegetation and environment at Cauduntou, west of Yangtze Delta, SW Jiangsu Province, East China. *Quat Int* 105:39–47. [https://doi.org/10.1016/S1040-6182\(02\)00149-0](https://doi.org/10.1016/S1040-6182(02)00149-0)
- Pausata FSR, Battisti DS, Nisancioglu KH, Bitz CM (2011) Chinese stalagmite  $[\delta^{18}O]$  controlled by changes in the Indian monsoon during a simulated Heinrich event. *Nat Geosci* 4:474–480. <https://doi.org/10.1038/ngeo1169>
- Peel MC, Finlayson BL, McMahon TA (2007) Updated world map of the Köppen–Geiger climate classification. *Hydrol Earth Syst Sci Discuss* 4:439–473
- Peltier WR (2004) GLOBAL GLACIAL ISOSTASY AND THE SURFACE OF THE ICE-AGE EARTH: the ICE-5G (VM2) Model and GRACE. *Ann Rev Earth Planet Sci* 32:111–149. <https://doi.org/10.1146/annurev.earth.32.082503.144359>
- Prentice IC (1980) Multidimensional scaling as a research tool in quaternary palynology: a review of theory and methods. *Rev Palaeobot Palynol* 31:71–104. [https://doi.org/10.1016/0034-6667\(80\)90023-8](https://doi.org/10.1016/0034-6667(80)90023-8)
- Reimer PJ et al (2013) IntCal13 and Marine13 radiocarbon age calibration curves 0–50,000 years cal BP. *Radiocarbon* 55(4):1869–1887
- Renssen H, Seppä H, Crosta X, Goosse H, Roche DM (2012) Global characterization of the Holocene thermal maximum. *Quat Sci Rev* 48:7–19. <https://doi.org/10.1016/j.quascirev.2012.05.022>
- Saraswat R, Lea DW, Nigam R, Mackensen A, Naik DK (2013) Deglaciation in the tropical Indian Ocean driven by interplay between the regional monsoon and global teleconnections. *Earth Planet Sci Lett* 375:166–175. <https://doi.org/10.1016/j.epsl.2013.05.022>
- Schneider T, Bischoff T, Haug GH (2014) Migrations and dynamics of the intertropical convergence zone. *Nature* 513:45–53. <https://doi.org/10.1038/nature13636>
- Shakun JD et al (2012) Global warming preceded by increasing carbon dioxide concentrations during the last deglaciation. *Nature* 484:49–54. <https://doi.org/10.1038/nature10915>
- Shanahan TM et al (2015) The time-transgressive termination of the African humid period. *Nat Geosci* 8:140. <https://doi.org/10.1038/ngeo2329>
- Shen J, Xingqi L, Sumin W, Matsumoto R (2005) Palaeoclimatic changes in the Qinghai Lake area during the last 18,000 years. *Quat Int* 136:131–140. <https://doi.org/10.1016/j.quaint.2004.11.014>
- Sheng M, Wang X, Zhang S, Chu G, Su Y, Yang Z (2017) A 20,000-year high-resolution pollen record from Huguangyan Maar Lake in tropical–subtropical South China. *Palaeogeogr Palaeoclimatol Palaeoecol* 472:83–92. <https://doi.org/10.1016/j.palaeo.2017.01.038>
- Shu J, Wang W, Chen W (2007) Holocene vegetation and environment changes in the NW Taihu plain, Jiangsu Province, East China. *Acta Micropalaeontol Sin* 24:210–221
- Song J, He J, Zhou L, Li F, Jiang S (1997) 1993–95 Excavations at the site of Maqiao in minhang district, Shanghai City. *Acta Archaeol Sin* 2:197–236
- Stebich M, Rehfeld K, Schlütz F, Tarasov PE, Liu J, Mingram J (2015) Holocene vegetation and climate dynamics of NE China based on the pollen record from Sihailongwan Maar Lake. *Quat Sci Rev* 124:275–289. <https://doi.org/10.1016/j.quascirev.2015.07.021>
- Stott L, Cannariato K, Thunell R, Haug GH, Koutavas A, Lund S (2004) Decline of surface temperature and salinity in the western tropical Pacific Ocean in the Holocene epoch. *Nature* 431:56–59. <https://doi.org/10.1038/nature02903>
- Sun Y, Clemens SC, Morrill C, Lin X, Wang X, An Z (2012) Influence of Atlantic meridional overturning circulation on the East Asian winter monsoon. *Nat Geosci* 5:46–49. <https://doi.org/10.1038/ngeo1326>
- Sun Y et al (2015) Astronomical and glacial forcing of East Asian summer monsoon variability. *Quat Sci Rev* 115:132–142. <https://doi.org/10.1016/j.quascirev.2015.03.009>

- Tan M (2014) Circulation effect: response of precipitation  $\delta^{18}O$  to the ENSO cycle in monsoon regions of China. *Clim Dyn* 42:1067–1077
- Telford RJ, Birks HJB (2011) A novel method for assessing the statistical significance of quantitative reconstructions inferred from biotic assemblages. *Quat Sci Rev* 30:1272–1278. <https://doi.org/10.1016/j.quascirev.2011.03.002>
- Teller JT, Leverington DW, Mann JD (2002) Freshwater outbursts to the oceans from glacial Lake Agassiz and their role in climate change during the last deglaciation. *Quat Sci Rev* 21:879–887. [https://doi.org/10.1016/S0277-3791\(01\)00145-7](https://doi.org/10.1016/S0277-3791(01)00145-7)
- Ter Braak CJF, Juggins S (1993) Weighted averaging partial least squares regression (WA-PLS): an improved method for reconstructing environmental variables from species assemblages. In: van Dam H (ed) Twelfth International Diatom Symposium: Proceedings of the twelfth international diatom symposium, Renesse, The Netherlands, 30 August–5 September 1992. Springer Netherlands, Dordrecht, pp 485–502. [https://doi.org/10.1007/978-94-017-3622-0\\_49](https://doi.org/10.1007/978-94-017-3622-0_49)
- Ter Braak CJ, Smilauer P (2002) CANOCO reference manual and CanoDraw for Windows user's guide: software for canonical community ordination (version 4.5). <http://www.canoco5.com/>. Accessed 16 Mar 2018
- van der Voet H (1994) Comparing the predictive accuracy of models using a simple randomization test. *Chemom Intell Lab Syst* 25:313–323. [https://doi.org/10.1016/0169-7439\(94\)85050-X](https://doi.org/10.1016/0169-7439(94)85050-X)
- Wang B (2006) The Asian monsoon. Springer, Berlin
- Wang FX, Qian NF, Zhang YL (1995) Pollen flora of China. Science Press, Beijing
- Wang B, Wu R, Fu X (2000) Pacific–East Asian teleconnection: how does ENSO affect East Asian climate? *J Clim* 13:1517–1536
- Wang YJ, Cheng H, Edwards RL, An ZS, Wu JY, Shen C-C, Dorale JA (2001) A high-resolution absolute-dated late pleistocene monsoon record from Hulu cave, China. *Science* 294:2345–2348. <https://doi.org/10.1126/science.1064618>
- Wang Y et al (2005) The Holocene Asian monsoon: links to solar changes and north Atlantic. *Clim Sci* 308:854–857. <https://doi.org/10.1126/science.1106296>
- Wang S, Lü H, Liu J, Negendank JFW (2007) The early Holocene optimum inferred from a high-resolution pollen record of Huguangyan Maar Lake in southern China. *Chin Sci Bull* 52:2829–2836. <https://doi.org/10.1007/s11434-007-0419-2>
- Wang B, Wu Z, Li J, Liu J, Chang C-P, Ding Y, Wu G (2008) How to measure the strength of the East Asian Summer Monsoon. *J Clim* 21:4449–4463. <https://doi.org/10.1175/2008JCLI2183.1>
- Wang B, Liu J, Kim H-J, Webster PJ, Yim S-Y (2012) Recent change of the global monsoon precipitation (1979–2008). *Clim Dyn* 39:1123–1135. <https://doi.org/10.1007/s00382-011-1266-z>
- Wang N, Zhang X, Jin L (2015) The spatial and temporal variation characteristics of the south Asia high and western Pacific subtropical high on millennial time scale. *Quat Sci* 35:1425–1436
- Weldeab S, Lea DW, Oberhänsli H, Schneider RR (2014) Links between southwestern tropical Indian Ocean SST and precipitation over southeastern Africa over the last 17kyr. *Palaeogeogr Palaeoclimatol Palaeoecol* 410:200–212. <https://doi.org/10.1016/j.palaeo.2014.06.001>
- Wen R, Xiao J, Chang Z, Zhai D, Xu Q, Li Y, Itoh S (2010) Holocene precipitation and temperature variations in the East Asian monsoonal margin from pollen data from Hulun Lake in northeastern Inner Mongolia, China. *Boreas* 39:262–272. <https://doi.org/10.1111/j.1502-3885.2009.00125.x>
- Wu ZY (1980) The vegetation of China. Science Press, Beijing
- Wu W, Liu T (2004) Possible role of the “Holocene Event 3” on the collapse of Neolithic Cultures around the Central Plain of China. *Quat Int* 117:153–166. [https://doi.org/10.1016/S1040-6182\(03\)00125-3](https://doi.org/10.1016/S1040-6182(03)00125-3)
- Wu L, Li F, Zhu C, Li L, Li B (2012a) Holocene environmental change and archaeology Yangtze River Valley China: review prospects. *Geosci Front* 3:875–892. <https://doi.org/10.1016/j.gsf.2012.02.006>
- Wu X, Zhang Z, Xu X, Shen J (2012b) Asian summer monsoonal variations during the Holocene revealed by Huguangyan maar lake sediment record. *Palaeogeogr Palaeoclimatol Palaeoecol* 323–325:13–21. <https://doi.org/10.1016/j.palaeo.2012.01.020>
- Xiao J, Xu Q, Nakamura T, Yang X, Liang W, Inouchi Y (2004) Holocene vegetation variation in the Daihai Lake region of north-central China: a direct indication of the Asian monsoon climatic history. *Quat Sci Rev* 23:1669–1679 doi. <https://doi.org/10.1016/j.quascirev.2004.01.005>
- Xiao J, Lü H, Zhou W, Zhao Z, Hao R (2007) Evolution of vegetation and climate since the last glacial maximum recorded at Dahu peat site South China. *Sci China Ser D Earth Sci* 50:1209–1217. <https://doi.org/10.1007/s11430-007-0068-y>
- Xiao J, Fan J, Zhai D, Wen R, Qin X (2015) Testing the model for linking grain-size component to lake level status of modern clastic lakes. *Quat Int* 355:34–43. <https://doi.org/10.1016/j.quaint.2014.04.023>
- Xie S et al (2013) Concordant monsoon-driven postglacial hydrological changes in peat and stalagmite records and their impacts on prehistoric cultures in central China. *Geology* 41:827–830. <https://doi.org/10.1130/g34318.1>
- Xu X, Chang WY, Liu J (1995) Changes in vegetation and climate in the Taihu Lake basin during the last 11 000 years. *Acta Palaeontol Sin* 35:175–186
- Xu J, Holbourn A, Kuhnt W, Jian Z, Kawamura H (2008) Changes in the thermocline structure of the Indonesian outflow during terminations I and II. *Earth Planet Sci Lett* 273:152–162. <https://doi.org/10.1016/j.epsl.2008.06.029>
- Xu Q, Xiao J, Li Y, Tian F, Nakagawa T (2010) Pollen-based quantitative reconstruction of holocene climate changes in the Daihai Lake Area, Inner Mongolia, China. *J Clim* 23:2856–2868. <https://doi.org/10.1175/2009jcli3155.1>
- Yang F, Lau KM (2004) Trend and variability of China precipitation in spring and summer: linkage to sea-surface temperatures. *Int J Climatol* 24:1625–1644. <https://doi.org/10.1002/joc.1094>
- Yang X, Wang S, Tong G (1996) Character of palynology and changes of monsoon climate over the last 10000 years in Gucheng Lake, Jiangsu Province. *Acta Botan Sin* 38:576–581
- Yang Q-S, Xing Y-W, Zhou Z-K (2009) Modern geographical distribution of *Tsuga* and its climatic conditions in the Asian monsoon region. *Acta Botan Yunnanica* 31:389–398
- Yang S, Ding Z, Li Y, Wang X, Jiang W, Huang X (2015a) Warming-induced northwestward migration of the East Asian monsoon rain belt from the Last Glacial Maximum to the mid-Holocene. *Proc Natl Acad Sci* 112:13178–13183 <https://doi.org/10.1073/pnas.1504688112>
- Yang X et al (2015b) Groundwater sapping as the cause of irreversible desertification of Hunshandake Sandy Lands, Inner Mongolia, northern China. *Proc Natl Acad Sci* 112:702–706 <https://doi.org/10.1073/pnas.1418090112>
- Yao F et al (2017a) Holocene climate change in the western part of Taihu Lake region, East China. *Palaeogeogr Palaeoclimatol Palaeoecol*. <https://doi.org/10.1016/j.palaeo.2017.08.022>
- Yao S, Jiang D, Fan G (2017b) Seasonality of precipitation over China. *Chin J Atmos Sci* 41(6):1191–1203 (**in Chinese with English abstract**)
- Yi S, Saito Y, Yang D-Y (2006) Palynological evidence for Holocene environmental change in the Changjiang (Yangtze River) Delta, China. *Palaeogeogr Palaeoclimatol Palaeoecol* 241:103–117. <https://doi.org/10.1016/j.palaeo.2006.06.016>

- Yu S-Y et al (2010) Freshwater outburst from Lake Superior as a trigger for the cold event 9300 years ago. *Science* 328:1262–1266. <https://doi.org/10.1126/science.1187860>
- Yuan D et al (2004) Timing, duration, and transitions of the last interglacial Asian monsoon. *Science* 304:575–578. <https://doi.org/10.1126/science.1091220>
- Zhang X, Jin L, Chen J, Lu H, Chen F (2017) Lagged response of summer precipitation to insolation forcing on the northeastern Tibetan Plateau during the Holocene. *Clim Dyn*. <https://doi.org/10.1007/s00382-017-3784-9>
- Zhao Y, Yu Z (2012) Vegetation response to Holocene climate change in East Asian monsoon-margin region. *Earth Sci Rev* 113:1–10. <https://doi.org/10.1016/j.earscirev.2012.03.001>
- Zhao Y, Yu Z, Chen F, Zhang J, Yang B (2009) Vegetation response to Holocene climate change in monsoon-influenced region of China. *Earth Sci Rev* 97:242–256
- Zhao P, Yang S, Yu R (2010) Long-term changes in rainfall over eastern china and large-scale atmospheric circulation associated with recent global warming. *J Clim* 23:1544–1562. <https://doi.org/10.1175/2009jcli2660.1>
- Zhao L et al (2017) Holocene vegetation dynamics in response to climate change and human activities derived from pollen and charcoal records from southeastern China. *Palaeogeogr Palaeoclimatol*. <https://doi.org/10.1016/j.palaeo.2017.06.035>
- Zheng Z et al (2008) Comparison of climatic threshold of geographical distribution between dominant plants and surface pollen in China. *Sci China Ser D Earth Sci* 51:1107–1120
- Zheng Z et al (2014) East Asian pollen database: modern pollen distribution and its quantitative relationship with vegetation and climate. *J Biogeogr* 41:1819–1832. <https://doi.org/10.1111/jbi.12361>
- Zhou W, Yu X, Jull AJT, Burr G, Xiao JY, Lu X, Xian F (2004) High-resolution evidence from southern China of an early Holocene optimum and a mid-Holocene dry event during the past 18,000 years. *Quat Res* 62:39–48 doi. <https://doi.org/10.1016/j.yqres.2004.05.004>
- Zhu S, Lu Q, Chen Y, Xi J, Sun Y (1987) Characteristics of Holocene sedimentary provinces in Shanghai region Recent Yangtze Delta Deposits. East China Normal University Press, Shanghai, pp 158–173
- Zhu C, Zheng C, Ma C, Yang X, Gao X, Wang H, Shao J (2003) On the Holocene sea-level highstand along the Yangtze Delta and Ning-shao Plain. *East China Chinese Science Bulletin* 48:2672–2683. <https://doi.org/10.1007/BF02901755>
- Zhu C, Ma C, Yu S-Y, Tang L, Zhang W, Lu X (2010) A detailed pollen record of vegetation and climate changes in Central China during the past 16,000 years. *Boreas* 39:69–76. <https://doi.org/10.1111/j.1502-3885.2009.00098.x>
- Zhu C et al (2014) Research progress on Holocene environmental archaeology in the Yangtze River Valley, China. *Acta Geogr Sin* 69:1268–1283
- Zhu Z, Feinberg JM, Xie S, Bourne MD, Huang C, Hu C, Cheng H (2017) Holocene ENSO-related cyclic storms recorded by magnetic minerals in speleothems of central China. *Proc Natl Acad Sci* 114:852–857. <https://doi.org/10.1073/pnas.1610930114>
- Zong Y, Chen Z, Innes JB, Chen C, Wang Z, Wang H (2007) Fire and flood management of coastal swamp enabled first rice paddy cultivation in east China. *Nature* 449:459
- Zuo X et al (2017) Dating rice remains through phytolith carbon-14 study reveals domestication at the beginning of the Holocene. *Proc Natl Acad Sci* 114:6486–6491. <https://doi.org/10.1073/pnas.1704304114>